https://doi.org/10.5194/acp-2020-979
Preprint. Discussion started: 22 October 2020

Atmospheric Chemistry and Physics Discussions

Effect of volcanic emissions on clouds during the 2008 and 2018 Kilauea degassing events

Katherine H. Breen[1, 2], Donifan Barahona[1], Tianle Yuan[1, 3], Huisheng Bian[1, 3], and Scott C. James[4]

[1]NASA, Goddard Space Flight Center, Greenbelt, MD, USA
[2]Universities Space Research Association, Columbia, MD, USA
[3]Joint Center for Earth Systems Technology. University of Maryland, Baltimore County, MD, USA
[4]Baylor University, Departments of Geosciences and Mechanical Engineering, Waco, TX, USA

Correspondence: Donifan Barahona (donifan.o.barahona@nasa.gov)

Abstract.

Aerosol emissions from volcanic eruptions in otherwise clean environments are regarded as "natural experiments" where the aerosol effects on clouds and climate can be partitioned from other effects like meteorology and anthropogenic emissions. In this work, we combined satellite retrievals, reanalysis products, and atmospheric modeling to analyze the mechanism of aerosol-cloud interactions during two degassing events at the Kilauea Volcano in 2008 and 2018. The eruptive nature of the 2008 and 2018 degassing events was distinct from long-term volcanic activity for Kilauea. For both events, we performed a comprehensive investigation on the effects of aerosol emissions on macro and microphysical cloud processes for both liquid and ice clouds. This is the first time such an analysis has been reported for the 2018 event. Similarities between both events suggested that aerosol-cloud interactions related to the cloud albedo modification were likely decoupled from local meteorology. In both events the ingestion of aerosols within convective parcels enhanced the detrainment of condensate in the upper troposphere resulting in deeper clouds than in pristine conditions. Accounting for ice nucleation on ash particles led to enhanced ice crystal concentrations at cirrus levels and a slight decrease in ice water content, improving the correlation of the model results with the satellite retrievals. Overall, aerosol loading, plume characteristics, and meteorology contributed to observed and simulated changes in clouds during the Kilauea degassing events.

1 Introduction

Aerosol emissions influence Earth's climate both directly and indirectly. The direct effect involves scattering and absorption of thermal and solar radiation by atmospheric aerosols, while indirect effects involve alteration of the microphysical properties and the global distribution of clouds (Boucher et al., 2013; Twomey, 1977). Both liquid and ice clouds are susceptible to aerosol emissions that can alter their microphysical (i.e., particle size distribution and albedo) and macrophysical properties (liquid and ice water content, cloud lifetime, and cloud fraction) (Lohmann and Feichter, 2005; Boucher et al., 2013; Seinfeld et al., 2016). These effects, collectively known as aerosol indirect effects (AIEs), may offset a significant fraction of the warming induced by greenhouse gas emissions, yet their magnitudes are poorly constrained (Boucher et al., 2013).

https://doi.org/10.5194/acp-2020-979
Preprint. Discussion started: 22 October 2020


Atmospheric Chemistry and Physics Discussions

Because aerosol effects on clouds are difficult to partition from meteorological variability (i.e., variation in temperature, water vapor, and winds from large scale forcing) it has been challenging to develop observational signatures characteristic of AIEs (Lohmann and Feichter, 2005; Gryspeerdt et al., 2017). Satellite datasets facilitate global observational monitoring of meteorology, ambient aerosol concentration and distribution, and cloud properties. However, inferring aerosol–cloud interactions (ACIs) from satellite retrievals is difficult due to the concurrent influence of meteorological factors on clouds. From a modeling perspective, the relevant scale for ACIs (i.e., tens to hundreds of meters) is typically unresolved in atmospheric general circulation models (AGCMs; Boucher et al., 2013), where grid resolution is coarser (generally thousands of meters). The parameterization of ACIs in AGCMs is largely dependent on theory with many assumptions involved, and model outputs are difficult to validate directly against satellite retrievals due to differences in resolution.

The presence of cloud condensation nuclei, (CCN; typically sulfates, organics, and nitrate particles) in the atmosphere indirectly impacts Earth's net radiative balance by increasing the number of cloud droplets, hence altering the scattering and absorption of incoming solar radiation. This effect, historically referred to as the first AIE, or "Twomey" effect (Twomey, 1977), represents a change in the albedo of Earth's atmosphere and results in net radiative cooling. Smaller droplets are less efficient at coalescing into rain-bearing clouds, which is typically known as the second AIE (Albrecht, 1989). Non-precipitating clouds have a longer lifetime and thereby provide extended coverage, further enhancing Earth's albedo. Aerosols can also act as ice nucleation particles (INPs; typically dust, soot, and organics), modifying cloud properties at low temperature (Lohmann and Feichter, 2005). Besides these effects, accumulated CCN (due to precipitation suppression in liquid clouds) and INP ascend within convective parcels determine, to a large extent, the onset of precipitation by modifying the release of latent heat within convective clouds at higher altitudes (Koren et al., 2005).

https://doi.org/10.5194/acp-2020-979
Preprint. Discussion started: 22 October 2020

Figure 1. © Google Earth imagery of the Kilauea summit crater before and after each degassing event. Clockwise from top left: Pre-2008 degassing; post-2008 degassing, during 2018 peak degassing, and post-2018 degassing. The image from June 5, 2011 shows the summit vent, which was not present prior to the 2008 event, passively degassing during an eruptive lull. The image from May 30, 2018 was taken on a cloudy day during the 2018 event, several days after peak observed sulfate emissions ($50\,\mathrm{kt\,day^{-1}}$) and plume height ($<8\,\mathrm{km}$) (Neal et al., 2019). The red boxes approximately outline the summit crater while the "X"s indicate the degassing vent.

Volcanic degassing events in otherwise "clean" environments, where anthropogenic aerosol emissions are minimal, have been used as "natural" experiments to identify characteristics of ACIs in satellite retrievals and to evaluate AIEs in AGCMs (Eguchi et al., 2011; Yuan et al., 2011; Beirle et al., 2014; Malavelle et al., 2017). In this work, we assess the effects of sulfate and ash aerosols on liquid and ice cloud formation during two volcanic degassing events from the Kilauea Volcano in June 2008 and May 2018 (Figure 1). In both of these events, atmospheric aerosol loading increased by several orders of magnitude over a few days and remained high for at least two to three months. The background influx of SO_2 in this region is low due to seasonal atmospheric circulation and low-level anthropogenic pollution, therefore the surrounding atmosphere is relatively "clean," and the aerosols related to volcanic activity are independent of air mass processes. Emission rates of SO_2 during the 2018 event were conservatively $\geq 5\times$ higher than 2008 peak degassing emissions (Neal et al., 2019; Elias and Sutton, 2012) (Fig. 2). Whereas several studies have focused on the 2008 event (Eguchi et al., 2011; Yuan et al., 2011; Beirle et al., 2014; Malavelle et al., 2017), this is the first time that the impact of the 2018 event on cloud evolution has been analyzed.

https://doi.org/10.5194/acp-2020-979
Preprint. Discussion started: 22 October 2020

Atmospheric Chemistry and Physics Discussions

1.1 Kilauea degassing events

Kilauea is an active basaltic shield volcano located on the Island of Hawai'i. For the past 200 years, volcanic activity at Kilauea has been characterized by weak eruptive (explosive) and effusive (lava-flow) events that can continue for hours to months or even years at a time. The Halemaumau summit crater has been active since 1924 from which relatively small eruptive events are common, while effusive fissure eruptions have dominated the eastern rift zone (ERZ) on Kilauea's eastern flank in the historical record. Since March 2008, volcanic activity on Kilauea has been marked by summit degassing and flank eruptions with increasing intensity and frequency (Nadeau et al., 2015). Volcanic plumes on Kilauea are generally low-altitude ($< 10\,\mathrm{km}$) due to the gentle slopes of the volcano providing little protection from strong trade winds and the depth of the summit crater ($< 100\,\mathrm{m}$) (Elias et al., 2018).

1.1.1 The 2008 degassing event

Beginning in June 2007, an increase in volcanic activity was observed at the summit and ERZ of the Kilauea Volcano. This activity was characterized by brief summit eruptions followed by effusive ERZ fissure activity, which produced a diffuse, multi-source plume of SO_2. Between September and March 2008, lava pooled in a widening vent at the Halemaumau summit crater, followed by a brief explosive eruption. From March 2008 through December 2010, summit activity was characterized by degassing bursts from lava in the enlarging vent cavity, small explosive events, and eruptive pauses in December 2008 and July 2009. During degassing events, the estimated SO_2 plume height ranged from 1,200 to 2,500 m above sea level and SO_2 emissions exceeded 1,000 tonnes per day (Elias and Sutton, 2012). Degassing events produced variable volumes of tephra (ash), although larger explosive events, such as the initial summit eruption in March 2008, scattered lithic material (rock and ash) as much as 50 ha surrounding the vent and produced an ash-rich plume (Elias and Sutton, 2012; Nadeau et al., 2015).

Figure 1 (top row) shows images before and after the 2008 degassing event. After the 2008 event, the vent can be seen in the SE corner of the summit crater passively degassing from the lava lake during an eruptive pause. Observational and modeling studies reveal a significant departure of cloud droplet size, fraction, and optical thickness from their climatological values during the 2008 event, consistent with increased concentrations of atmospheric aerosols within the SO_2 plume from the Kilauea summit crater (Eguchi et al., 2011; Yuan et al., 2011; Beirle et al., 2014; Mace and Abernathy, 2016; Malavelle et al., 2017). Notwithstanding, model comparisons with NASA's Moderate Resolution Imaging Spectroradiometer (MODIS) aerosol indices suggest weak effects on cloud fraction and liquid water path (Malavelle et al., 2017; Bender et al., 2019).

1.1.2 The 2018 eruptive event

Beginning in mid-March 2018, increased lava levels were observed in the summit crater (Neal et al., 2019). By May 2018, effusive and eruptive activity in the ERZ generated flows and fountains. Subsidence of the summit caldera and increased seismicity were observed coincident with increased volcanic activity. From mid- to late-May, small summit eruptions ejected lithic material and ash $\approx$ 2,000 m above the summit vent on several occasions. On May 17, an eruptive event created a plume of SO_2 and ash $\approx$ 8,100 m above the summit vent and SO_2 concentrations remained elevated (Neal et al., 2019). On May 27

https://doi.org/10.5194/acp-2020-979
Preprint. Discussion started: 22 October 2020


Atmospheric Chemistry and Physics Discussions

and 28, ERZ eruptive events (lava fountains $< 80\,\mathrm{m}$) were associated with SO_2 emissions of $\geq 50,000$ tonnes per day (Neal et al., 2019; Elias et al., 2018). Multiple cycles of ongoing short pulses of eruptive degassing activity at the vent and longer periods of effusive volcanism in the ERZ caused ongoing aerosol emissions (Patrick et al., 2019).

Figure 1 shows the summit crater before, during, and after peak eruptive activity and indicates optically denser clouds within the aerosol plume with respect to surrounding clouds during peak degassing (Figure 1, lower right). Aerosol optical depth, measurements of SO_2 emissions, and plume morphology (Neal et al., 2019) indicated that during the peak eruptive period from mid to late-May, aerosol plumes associated with the 2018 degassing event were high-altitude plumes of mixed composition (SO_2 and ash). Ash content was high during summit degassing eruptions and decreased as effusive activity dominated eruptive behavior until all activity abruptly stopped in early August 2018. The height and composition of the plume in 2018 were similar to more violent, siliclastic eruption types (i.e., Mt. St. Helens; Mastin et al., 2009), therefore the 2018 event was not typical for basaltic magmas characteristic of historic Kilauea eruptions.

2 Data

The MODIS Aqua Aerosol Cloud Monthly collection 6 L3 Global 1° datasets (MYD08_M3) were acquired from the Level-1 and Atmosphere Archive & Distribution System (LAADS) Distributed Active Archive Center (DAAC) (https://ladsweb.nascom.nasa.gov/). The MODIS CDNC climatology (2003 – 2015) was obtained from Bennartz and Rausch (2017). MODIS CDNC data for 2018 were calculated using the method of Bennartz (2007). Gridbox mean LWP and IWP were calculated by scaling the MODIS product using the retrieved liquid and ice cloud fractions, respectively. No significant differences were found by scaling using either daily data (MYD08_D3) aggregated into monthly means (Malavelle et al., 2017) or monthly products (MYD08_M3), therefore monthly MODIS products were used in the analysis. MODIS anomalies were calculated as the 3-month average during peak degassing minus the long-term mean (2003–2015, excepting 2008). Missing values in MODIS data, primarily found in CDNC and ice products, were smoothed usign a gaussian filter.

NASA's Cloud-Aerosol Lidar and Infrared Pathfinder Satellite Observation (CALIPSO) instrument probes vertical cloud structures and provides 3-D perspectives of ACIs. The CALIPSO-GCM Oriented Cloud CALIPSO Product (CALIPSO-GOCCP) is a satellite data product developed with CALIPSO L1 data at full horizontal resolution (330 m) and vertical resolution typical for most GCMs (Chepfer et al., 2010). The dataset may be used for comparison either directly to AGCM output or to AGCM and LiDAR-simulator output, and is comparable to other standard cloud fraction climatologies (Chepfer et al., 2010).

3 GEOS model description

The NASA's Global Earth Observing System (GEOS), version 5, was used to analyze and understand the observed modification to cloud properties during the 2008 and 2018 Kilauea events (Barahona et al., 2014; Molod et al., 2015). GEOS consists of a set of components that numerically represent different aspects of the Earth system (atmosphere, ocean, land, sea-ice and

https://doi.org/10.5194/acp-2020-979
Preprint. Discussion started: 22 October 2020

Atmospheric Chemistry and Physics Discussions

chemistry), coupled following the Earth System Modeling Framework (https://gmao.gsfc.nasa.gov/GEOS_systems/). For this work, the AGCM configuration of GEOS was used. Atmospheric transport of water vapor, condensate and other tracers, and associated land-atmosphere exchanges, was computed explicitly, whereas sea-ice and sea surface temperature (SST) were prescribed as time-dependent boundary conditions (Reynolds et al., 2002; Rienecker et al., 2008).

Transport of aerosols and gaseous tracers such as CO were simulated using the Goddard Chemistry Aerosol and Radiation model (GOCART) (Colarco et al., 2010), which explicitly calculates the transport and evolution of dust, black carbon, organic material, sea salt, and sulfate. Dust and sea salt emissions are prognostic whereas sulfate and biomass burning emissions were obtained from the Modern Era Retrospective Reanalysis for Research and Applications-Version 2 (MERRA-2) reanalysis dataset (Randles et al., 2017). Volcanic SO_2 emissions are constrained by observations from the Ozone Monitoring Instrument (OMI) on-board NASA's EOS/Aura spacecraft (Carn et al., 2015). For the Kilauea volcano, this dataset only provides "constant" annual SO^2 emission rates. For the two events (2008 and 2018) we replaced this data set with daily varying emissions (Carn et al., 2017). The altitude of the Kilauea summit crater is $\approx 1200\,\mathrm{m}$, while the well-mixed boundary layer tops are around 2 km. For this reason, we allow the degassing volcano emission to be distributed within 1 km above the summit crater.

Cloud microphysics is described using a two-moment scheme where the mixing ratio and number concentration of cloud droplets and ice crystals are prognostic variables (Barahona et al., 2014; Morrison and Gettelman, 2008). The two-moment microphysical model links aerosol emissions to cloud properties and predicted the mixing ratio, number concentration, and effective radius of cloud liquid and ice, rain, and snow for stratiform clouds i.e., cirrus, stratocumulus (Morrison and Gettelman, 2008), and convective clouds (Barahona et al., 2014). Cloud droplet activation is parameterized using the approach of Abdul-Razzak and Ghan (2000). Ice crystal nucleation is described using a physically-based analytical approach (Barahona and Nenes, 2009a) that included homogeneous and heterogeneous ice nucleation, and their competition. Heterogeneous ice nucleation in the immersion and deposition modes follows Ullrich et al. (2017). Vertical velocity fluctuations were constrained by non-hydrostatic, high-resolution global simulations (Barahona et al., 2017). Using this configuration, GEOS reproduces the global distribution of clouds, radiation, and precipitation in agreement with satellite retrievals and *in situ* observations (Barahona et al., 2014).

Typically, a model run "drifts" toward its own climate, making it difficult to compare to observations. To correct for this, all simulations were run in "replay" mode, where analysis increments from MERRA-2 were combined with the model results to generate new analysis increments, and then applied to correct the model state every six hours. The replay technique is more stable and has lower numerical drift than regular nudging (Takacs et al., 2018). Temperature and horizontal winds were replayed to the MERRA-2 reanalysis. However, because the two-moment cloud scheme used in this work differed from the single-moment scheme used in MERRA-2, water vapor was left to evolve with the model physics. Running in replay mode ensured that the effects of meteorological variability were reduced and that our simulations reproduced the assimilated atmospheric state as closely as possible. Replaying temperature (T) also minimized the role of direct and semi-direct effects in modifying cloud properties. Hence, our analysis focuses on the evolution of cloud microphysical properties. On the other hand, because T was constrained (although water vapor evolves freely), cloud adjustments (i.e., the second AIE) were only partially represented.

https://doi.org/10.5194/acp-2020-979
Preprint. Discussion started: 22 October 2020


Atmospheric Chemistry and Physics Discussions

4 Methods

To help explain the observed changes in cloud properties during the 2008 and 2018 Kilauea degassing events, and to what these changes were sensitive to, we undertook a set of AGCM numerical experiments (Table 1) constrained by observed SO_2 emissions (Carn et al., 2015) and by MERRA-2 (Gelaro et al., 2017). Our objective was to generate a close representation of the clouds formed during each event to understand how aerosol emissions impacted cloud microphysics and evolution.

4.0.1 Description of simulation experiments

We performed several global integrations of GEOS to best isolate the effects of volcanic aerosol emissions on cloud development. Each simulation was initialized on January 1st of each year, and run at a nominal horizontal resolution of 0.5°with 72 vertical levels. The time step was set to $450\,\mathrm{s}$ to resolve the large scale transport of aerosol and condensate. Cloud microphysics was sub-cycled twice each time step to account for unresolved, fast microphysical processes such as CCN activation (Morrison and Gettelman, 2008). For each event, control runs (identified as 1×, Table 1) used the default model and emissions as described in Section 3. A second set of simulations was performed for each event removing the emissions from the Kilauea Volcano (0×) to represent background conditions unaffected by the degassing events. Sensitivity studies were also performed. A five-fold actual emissions run (2008_5×) was performed to compare the 2008 and 2018 events (the 2018 event emitted ≥ 5 times the aerosol load of the 2008 event) to assess the similarities between the events with respect to increased aerosol loading. Simulations to test the effect of sulfate and ash injection on cloud microphysics (i.e., the elevation where volcanic emissions were emitted from the model) were also performed (2008_PH2km and 2018_PH4km). Finally, another numerical experiment was carried out for the year 2018 (2018_PH4km_ash), where the effect of ash as active INP was investigated, as described in Appendix A. Besides these experiments, long-term model integration (2000–2017) was performed to represent the climatology of the models ($GEOS_{CLIM}$). The simulation experiments are summarized in Table 1.

4.1 Analysis Method

MODIS retrievals and the 1× GEOS experiments were compared against the long-term climatology excluding 2008 during peak degassing periods for each event. The 1× simulations were also compared against the 0× results for each year (1×−0×). In this way, we assessed the effects of volcanic aerosols on cloud formation separated from natural meteorological variability. This also allowed for the assessment of whether passive degassing effects present in $GEOS_{CLIM}$ were significant contributors to ACIs as opposed to active degassing events in 2008 and 2018. Anomalies for each degassing event were calculated as the seasonal mean during peak eruptive periods with long-term seasonal averages removed. We focused on the boreal summer (June-July-August, JJA) for the 2008 degassing event and the transition from the boreal spring to summer (May-June-July, MJJ) for 2018, when emissions from both events were highest and active eruptive events projecting ash and lithics into the volcanic plume occurred. To assess anomalies at the source relative to areas outside of the plume, normalized zonal mean

https://doi.org/10.5194/acp-2020-979
Preprint. Discussion started: 22 October 2020


Atmospheric Chemistry and Physics Discussions

Table 1. Simulation experiments performed.

Year	Experiment Name	Description
2008	2008_1X	Control simulation
	2008_0X	No emissions from Kilauea
	2008_5X	Five-fold increase in Kilauea emissions
	2008_PH2km	Volcanic plume height increased to 2 km
2018	2018_1X	Control simulation
	2018_0X	No emissions from Kilauea
	2018_PH4km	Volcanic plume height increased to 4 km
	2018_PH4kmAsh	2018_PH4km plus ice nucleation on ash particles
2000–2017	$\text{GEOS}_{\text{CLIM}}$	GEOS climatology excepting 2008

anomalies were calculated as

$$v_{\text{lat,norm}}(i) = \frac{v_{\text{lat}}(i)}{\sqrt{\sum_{i=1}^{N} v_{\text{lat}}(i)^2}}, \tag{1}$$

where N is the number of latitudes in the domain at 5°intervals (10°–25° N), $v_{\text{lat}}(i)$ is the seasonal latitudinal average (JJA 2008 or MJJ 2018) at latitude i, and $v_{\text{lat,norm}}(i)$ is the seasonal latitudinal anomaly normalized by the latitudinal mean (JJA or MJJ averaged over the climatology) at latitude i. To emphasize the location of the plume we focus on a domain that includes only areas west of the source ((25°,–155° NE),(10°,–180° SW)).

5 Results and Discussion

The goal of this work is to investigate the role of microphysical processes on ACIs during the Kilauea degassing events. To that end, we first show the reliability of our simulations by comparing satellite retrievals and GEOS control simulations (2008_1× and 2018_1×) and sensitivity experiments (2008_5×, 2018_PH4km, and 2018_PH4km_ash). We then look for common features to both the 2008 and 2018 Kilauea degassing events. Finally, Section 5.1 details the specific microphysical processes involved in cloud modification by the Kilauea emissions. Our results suggested that it is likely that the effect of volcanic emissions on cloud microphysics is specific to cloud phase. When possible, we divide the discussion between effects on ice and liquid clouds.

https://doi.org/10.5194/acp-2020-979
Preprint. Discussion started: 22 October 2020

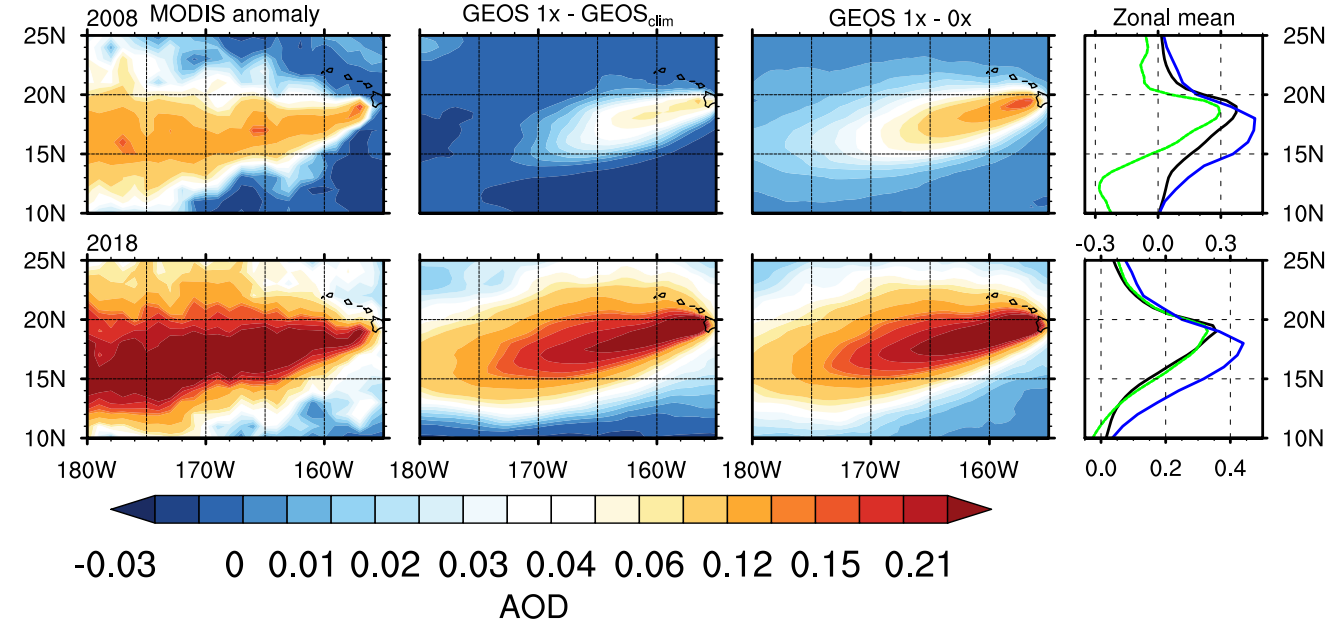

Figure 2. AOD anomalies (from left) for MODIS observations, and for GEOS simulations using actual emissions (2008_1x and 2018_1x) calculated against $GEOS_{CLIM}$ and the zero emissions scenarios (2008_0x and 2018_0x), during JJA 2008 (top) and MJJ 2018 (bottom). The rightmost column shows normalized zonal mean anomalies for MODIS (blue), and GEOS against $GEOS_{CLIM}$ (green) and zero emissions (black). The latitude of the Kilauea volcano is shown in magenta.

Aerosol optical depth (AOD) anomalies from MODIS during peak degassing periods are shown in Fig. 2 for JJA 2008 (top left) and MJJ 2018 (bottom left). Figure 2 also shows modeled AOD anomalies for simulations using actual emissions (2008_1×, 2018_1×) calculated against the simulated climatology ($GEOS_{CLIM}$) and with zero emissions scenarios (2008_0×, 2018_0×). Elevated aerosol loadings were apparent beginning at Kilauea (19.4° N, 155.2° W) and extended in a near-Gaussian plume westward across the domain shown in Fig. 2. AOD anomalies outside of the plume domain were negligible, supporting the idea that Kilauea is located in an otherwise "clean" environment, relatively untouched by anthropogenic aerosol emissions from North America or East Asia. During both events the elevated AOD anomalies observed by MODIS extended westward from Kilauea in the path of the Pacific easterly trade winds (Yuan et al., 2011). This is well reproduced in the GEOS results. AOD anomalies appear weaker compared to $GEOS_{CLIM}$ than against 0×, particularly near the Kilauea crater. This is due to the fact that there is always some passive degassing near the source, which would be represented in the climatology but not in the 0× experiment. Passive degassing is shown in Fig. 1, where a thin plume coming from the summit crater was evident during an eruptive pause in 2011, a year without a major volcanic event at the site.

Figure 3 shows MODIS retrievals and GEOS simulations of the cloud fraction (CF) anomalies during the two events. Peak anomalies during the 2018 event (Fig. 3; bottom) were approximately 2–3× greater than during the 2008 event (Fig. 3; top).

https://doi.org/10.5194/acp-2020-979
Preprint. Discussion started: 22 October 2020

Atmospheric Chemistry and Physics Discussions

In both cases, the 1×−GEOS$_{CLIM}$ difference (middle panels) reproduced the spatial distribution of the CF anomaly from the MODIS retrieval, whereas the 1×−0× differences tended to overestimate the anomaly in 2008 and underestimated it in 2018. In 2008 the normalized 1×−GEOS$_{CLIM}$ anomaly correlates well with MODIS (Table 3) whereas there was essentially no correlation between the 1×−0× anomaly and the retrieval, indicating that the observed CF anomaly was mainly driven by meteorological variability, likely differences in SST (Takahashi and Watanabe, 2016; Boo et al., 2015). Thus ACIs likely had only a minor effect on CF for the two degassing events. It is possible that the aerosol layer may have locally modified SST, hence indirectly affecting CF. Elucidating this requires coupled ocean-atmosphere simulations and is suggested for future research.

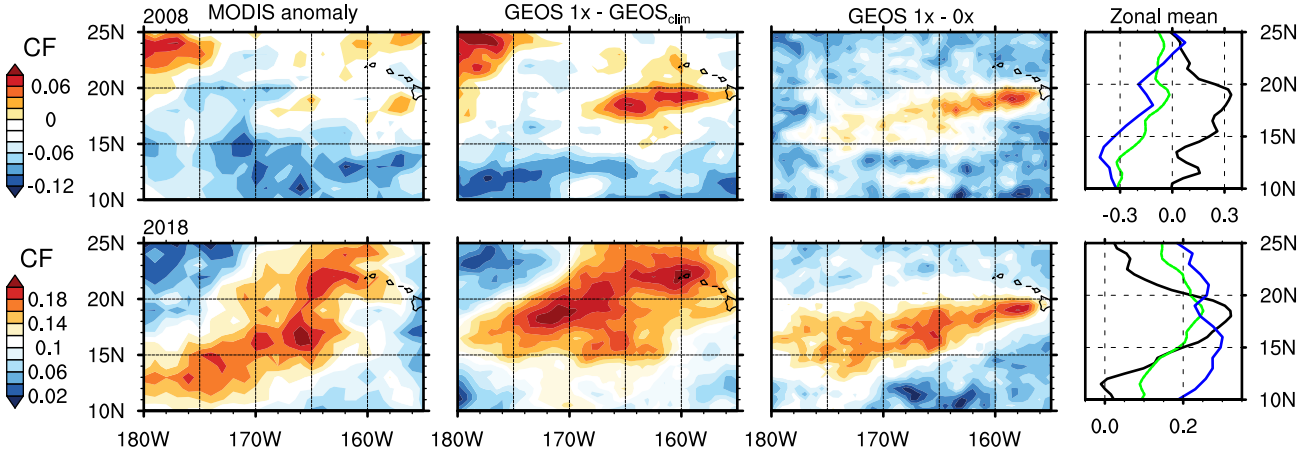

Figure 3. Like Fig.2 but showing cloud fraction anomalies during JJA 2008 (top) and MJJ 2018 (bottom).

To examine the cloud vertical structure during the two degassing events, GEOS results for the 2008_1× and 2018_1× simulations were compared against CALIPSO-GOCCP, shown in Figs. 4 and 5, respectively. During both events predominant cloud layers were found at 900 hPa and 200 hPa, corresponding to low-level trade cumulus and *in situ* formation of thin cirrus clouds, respectively. It is remarkable that the cloud vertical structure during both events was similar, indicating a strong meteorological control. This was well-captured by the GEOS simulations; the model however tended to overestimate high-level clouds and underestimate low-level clouds, particularly during the 2018 event (Fig. 5). Replaying temperature but letting water vapor evolve freely tends to produce spurious supersaturation, particularly at cirrus levels, where the two-moment microphysics allows for supersaturation but MERRA-2 does not, and T is less constrained by observations (Gelaro et al., 2017). On the other hand, it has been reported that GOCCP tends to underestimate the presence of thin cirrus clouds, and may overestimate low-level clouds in the presence of high aerosol loading (Chepfer et al., 2010). These factors add uncertainty to the CF retrievals. GEOS was however able to simulate an anomalous increase in CF above 800 hPa between 20°N and 25° N in 2008 as seen in the retrieval. Similarly, there was a strong increase in CF in 2018 across the domain, although GEOS predicted a much larger anomaly effect on cirrus clouds. Again, the discrepancy may be the result of a lack of sensitivity to thin cirrus clouds in GOCCP.

https://doi.org/10.5194/acp-2020-979
Preprint. Discussion started: 22 October 2020

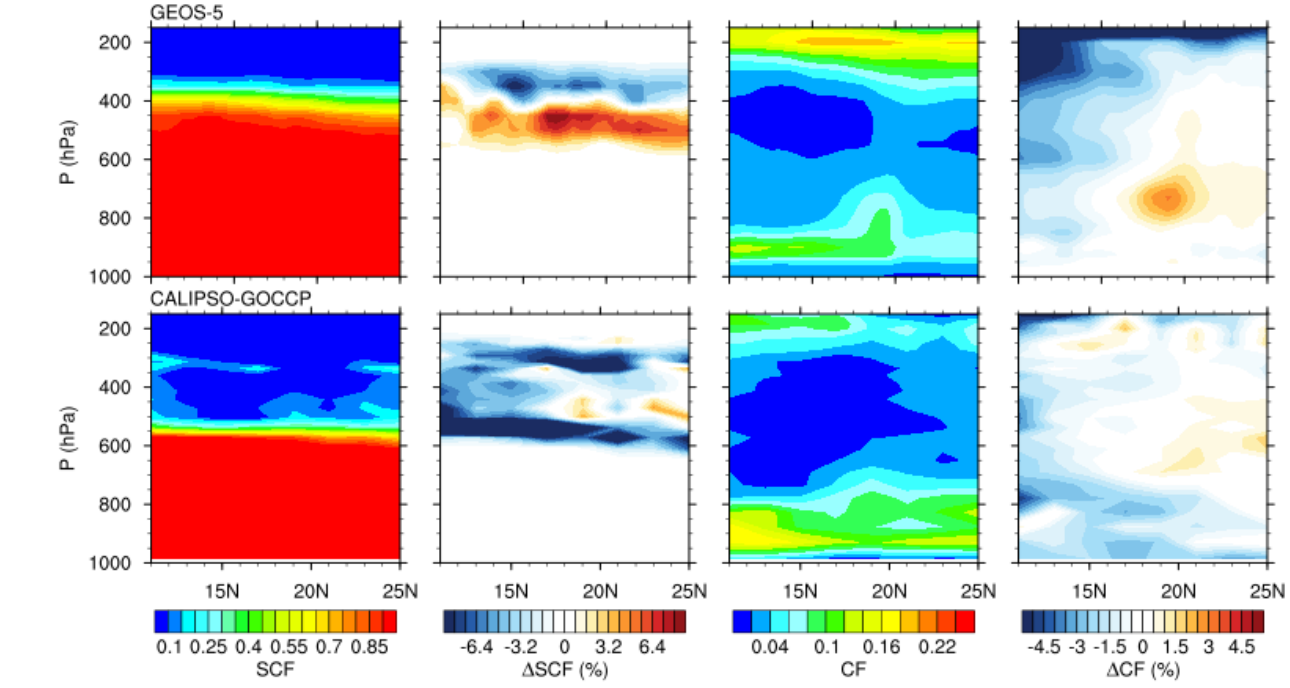

Figure 4. Zonal mean JJA supercooled cloud fraction (SCF) and cloud fraction from the GEOS (top) simulation and the CALIPSO-GOCCP (bottom) dataset. Also shown are the anomalies with respect to the 2007–2017 climatology (excluding 2008).

Another interesting feature of Figs. 4 and 5 is the presence of mid-level, alto-cumulus clouds likely maintaining some supercooled water. In GOCCP, the supercooled cloud fraction (SCF) (i.e., the fraction of condensate remaining as liquid at $T < 273$ K) decreased sharply at around 550 hPa in both years, but surprisingly remained low (≈ 0.1) up to 200 hPa where homogeneous ice nucleation glaciated the remaining water. This was particularly true in 2018 where GOCCP showed enhanced SCF relative to the climatology. GEOS showed similar behavior where the supercooled layer ($0 < \text{SCF} < 1$) was deeper in 2018 than in 2008, particularly near the summit crater ($\approx 25°$ N). The supercooled layer was almost $100\,\text{hPa}$ higher in GEOS than in GOCCP, indicating differences in ice and liquid partitioning between the model and the retrieval, and may be explained by the different definitions of SCF in each case. In GEOS, SCF is calculated on a mass basis, whereas in GOCCP it corresponds to the frequency of pixels that are classified as ice. The positive anomaly in SCF may suggest a deepening of the cloud in the presence of aerosol and is analyzed in Section 5.1.

5.0.1 Liquid Clouds

Figures 6 and 7 show anomalies in cloud effective radius (R_{eff}), droplet number concentration (CDNC), optical depth (COD), and liquid water path (LWP) for MODIS and the GEOS simulations (Table 1) during the 2008 and 2018 degassing events, respectively. Domain mean anomalies are summarized in Table 2. Student's *t*-test statistics indicated that the anomalies were

https://doi.org/10.5194/acp-2020-979
Preprint. Discussion started: 22 October 2020

Atmospheric Chemistry and Physics Discussions

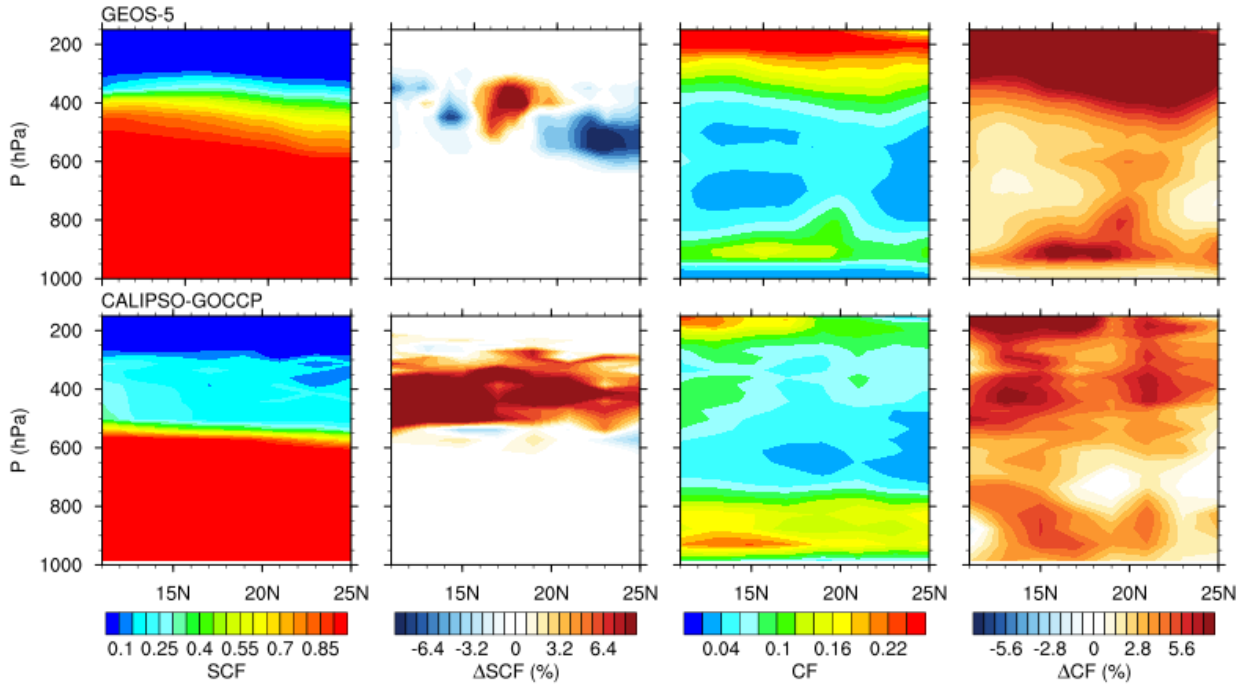

Figure 5. Like Figure 4 but for May-June-July, 2018.

statistically significant, typically to a 70%-80% level ($p < 0.3$) for R_{eff} and CDNC more so than for other variables. Additionally, we found that effects on liquid clouds were more statistically significant in 2018 than in 2008. In 2018 the magnitude and significance level of the anomalies against $GEOS_{CLIM}$ were close to those calculated against 2018_0× indicating that increased aerosol loading, regardless of injection height, resulted in the heightened development of liquid cloud droplets, and that these effects could be attributed to volcanic degassing as opposed to regional meteorology. The plume domain the results of the 2008_5× run were in general highly statistically significant ($p < 0.05$). This and the similarities in spatial patterns for cloud anomalies in JJA 2008 (Figure 6) and MJJ 2018 (Figure 7) suggested a threshold response to overcome meteorological effects that is largely controlled by emissions.

Table 3 shows the coefficient of determination (R^2) between the MODIS and the GEOS normalized zonal mean anomalies. Overall, more robust correlations ($R^2 > 0.5$) resulted when the anomalies were calculated against the $GEOS_{CLIM}$ than against the no-emissions scenarios. This indicated that while both GEOS climatology and 0× cases included aerosol loading consistent with MODIS retrievals (Figure 2, Table 3), correlations with observed data for liquid clouds were sensitive to meteorological effects captured by the MODIS and GEOS climatologies. MODIS TWP anomalies in 2018 were about 20× higher than those reported for the 2008 event (Table 2), suggesting that ACIs for 2018 were not limited to liquid clouds. During both the 2008 and the 2018 events, GEOS was able to capture the geographical distribution of the anomalies apparent in the MODIS retrievals. For the 2008_1× experiment, the magnitude of the R_{eff} ($-0.58\,\mu m$) and CDNC ($16.04\,cm^{-3}$) domain-averaged anomalies was

https://doi.org/10.5194/acp-2020-979
Preprint. Discussion started: 22 October 2020


Atmospheric Chemistry and Physics Discussions

in close agreement with MODIS ($-0.75\,\mu m$ and $21.53\,cm^{-3}$, respectively), and well-correlated with the satellite retrievals (Table 3). These values are also close to the anomalies calculated against the $2008\_0\times$ simulation suggesting a microphysical control to R_{eff} and CDNC. On the other hand, although the COD and LWP normalized anomalies are well-correlated between GEOS and MODIS, the model overestimates their absolute value. Similarly, in 2018 the GEOS and MODIS anomalies in R_{eff} ($-1.3\,\mu m$ vs. $-0.6\,\mu m$) and CDNC ($33.8\,cm^{-3}$ vs. $19.4\,cm^{-3}$) were in better agreement than for COD (9.25 vs. 0.69) and LWP ($17.84\,g\,m^{-2}$ vs. $5.09\,g\,m^{-2}$). Normalized zonal mean anomalies were, however, highly correlated (Table 3). The discrepancy in LWP and COD absolute anomalies was likely due to variation in SSTs inside the domain, and the lack of a cloud albedo-SST feedback in our simulations.

Sulfate emissions at the Mauna Loa Observatory (19.5° N, 155.6° W) peaked in JJA 2008 relative to the 1995–2008 seasonal mean, with prevailing La Niña conditions (Potter et al., 2013). Intensification of easterly trade winds could have increased transport of anthropogenic aerosols to the central tropical Pacific, although several volcanic eruptions in the Northern hemisphere, including the Kilauea 2008 event, contributed to elevated aerosol loadings. Thus it is likely that the degassing event contributed to lower SSTs, hence lower evaporation and LWP than would result only from microphysical processes. Replaying to analyzed temperatures would thus tend to result in a stronger response of clouds to aerosol loading in the model than in the retrieval. The negative anomaly in LWP in the southernmost part of the domain evident in 2008 is missing in the 2018 event due to neutral ENSO conditions in the latter (Team, Updated June 4, 2020 (accessed June 10, 2020). However, aerosol-SST feedback mechanisms may still limit the increase in LWP and COD from the aerosol loading. Thus, ENSO is a strong meteorological control that could "drown" out ACI signatures in both seasonal and long-term observations.

Another reason behind the larger aerosol effects on COD and LWP simulated by GEOS than observed by MODIS may lie in differences in phase partitioning (i.e., liquid vs. ice). To help identify thin cirrus clouds, measured Top-Of-the-Atmosphere (TOA) reflectance at 1.38 μm is used to partition high altitude cirrus clouds from low altitude liquid clouds. This method is strongly influenced by the relative humidity of the atmospheric column. Therefore, areas with low column water vapor amount may have more clouds partitioned to ice phase than is realistic. This is important because 2008 was a La Niña year and the relative humidity in the atmospheric column was lower than normal, so LWP anomalies may appear low because more clouds were partitioned to the ice phase in the MODIS cloud phase classification algorithm. Even in 2018, most of the total water path anomaly (TWP) results from an increase in the ice water path (Table 3).

https://doi.org/10.5194/acp-2020-979
Preprint. Discussion started: 22 October 2020

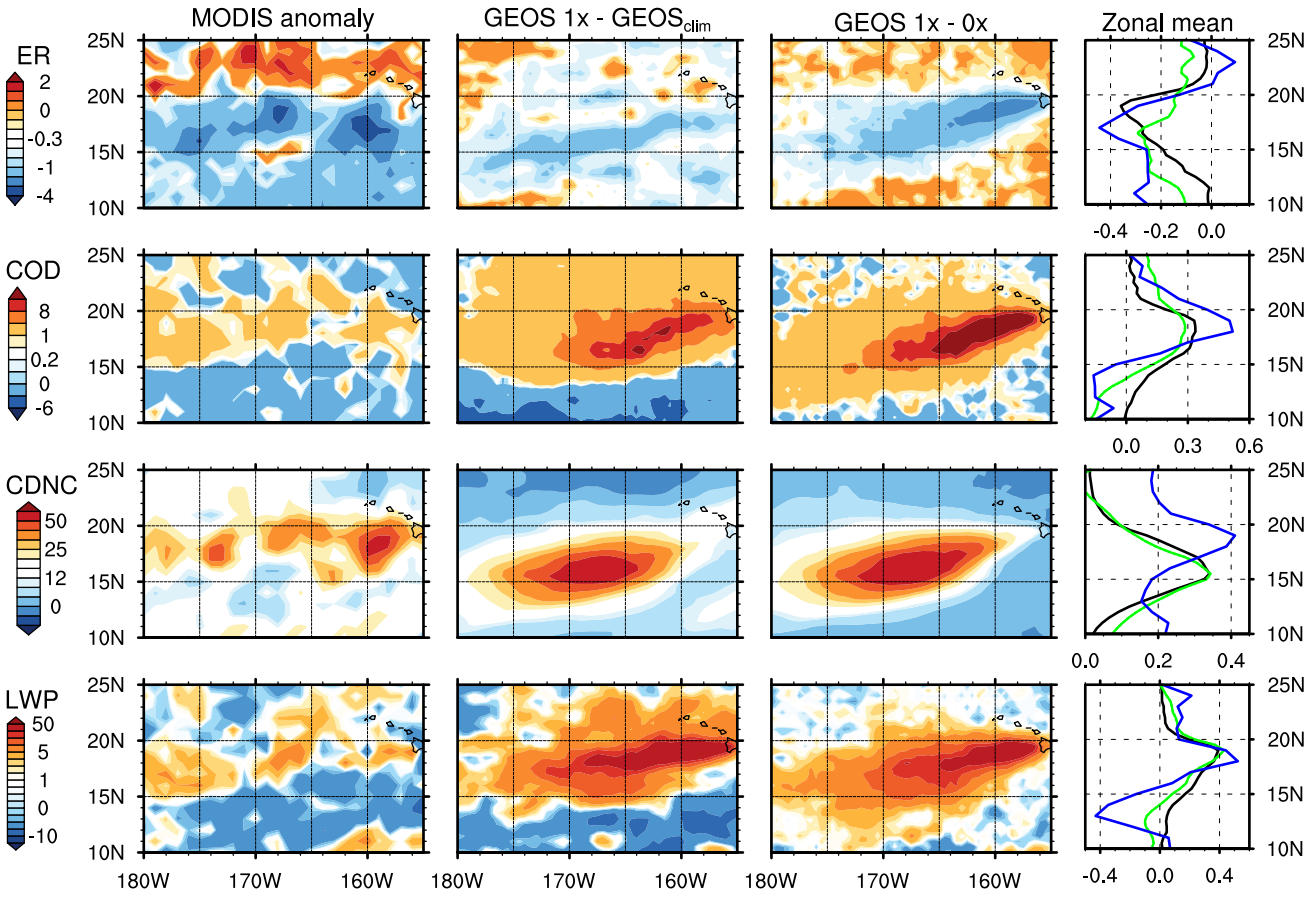

Figure 6. Anomaly in liquid cloud properties during JJA 2008 for (from top) R_{eff} (μm), COD, CDNC (m^{-3}), and LWP ($g\,m^{-2}$). Anomalies are shown (from left) for MODIS observations, and for GEOS simulations calculated against $GEOS_{CLIM}$ and the zero emissions scenario. The rightmost column shows normalized zonal mean anomalies for MODIS (blue), and GEOS against $GEOS_{CLIM}$ (green) and zero emissions (black).

https://doi.org/10.5194/acp-2020-979
Preprint. Discussion started: 22 October 2020

Atmospheric Chemistry and Physics Discussions

Table 2. Anomalies for liquid cloud properties, and for aerosol optical depth (AOD) and cloud fraction (CF). Values in parentheses are the p-values associated with a one-sided Student's t-test against the long-term mean.

Experiment	**Exp vs. climatology (excluding 2008)**							**Exp vs. 0×**						
	R_{eff} (μm)	COD (–)	CDNC (m^{-3})	LWP (g m^2)	TWP (g m^2)	AOD (–)	CF (–)	R_{eff} (μm)	COD (–)	CDNC (m^{-3})	LWP (g m^2)	TWP (g m^2)	AOD (–)	CF (–)
2008_1×	-0.58 (0.08)	4.63 (0.12)	16.04 (0.23)	8.77 (0.19)	8.31 (0.15)	0.01 (0.40)	-0.03 (0.41)	-0.65 (0.07)	3.77 (0.17)	15.68 (0.24)	6.82 (0.27)	7.17 (0.19)	0.03 (0.07)	0.02 (0.63)
2008_5×	-1.31 (0.01)	10.70 (0.02)	40.06 (0.01)	18.99 (0.05)	19.34 (0.02)	0.07 (0.07)	-0.01 (0.78)	-1.37 (0.01)	9.84 (0.02)	39.71 (0.01)	17.04 (0.06)	18.21 (0.02)	0.09 (0.04)	0.03 (0.32)
2008_PH2km	-0.58 (0.08)	4.63 (0.12)	16.04 (0.23)	8.77 (0.19)	8.70 (0.13)	0.01 (0.40)	-0.03 (0.41)	-0.45 (0.07)	2.31 (0.17)	13.55 (0.24)	4.03 (0.27)	4.90 (0.17)	0.02 (0.07)	0.01 (0.63)
MODIS (2008)	-0.75 (0.26)	0.46 (0.18)	21.53 (1.00)	0.65 (0.52)	-0.89 (0.74)	0.03 (0.04)	-0.02 (0.50)	– (–)	– (–)	– (–)	– (–)	– (–)	– (–)	– (–)
2018_1×	-1.33 (0.03)	9.25 (0.01)	33.86 (0.02)	17.84 (0.02)	49.29 (0.06)	0.10 (0.04)	0.16 (0.17)	-1.50 (0.02)	9.87 (0.01)	35.81 (0.02)	12.61 (0.04)	21.67 (0.22)	0.11 (0.04)	0.03 (0.73)
MODIS (2018)	-0.60 (0.14)	0.69 (0.24)	19.43 (0.02)	5.09 (0.21)	25.81 (0.23)	0.11 (0.00)	0.13 (0.20)	– (–)	– (–)	– (–)	– (–)	– (–)	– (–)	– (–)

Table 3. Linear coefficients of determination for the comparison of GEOS normalized zonal anomalies for liquid clouds against MODIS.

Experiment	**MODIS anomaly vs GEOS 1×−clim**							**MODIS anomaly vs GEOS 1×−0×**						
	R_{eff} (μm)	COD (–)	CDNC (m^{-3})	LWP (g m^2)	TWP (g m^2)	AOD (–)	CF (–)	R_{eff} (μm)	COD (–)	CDNC (m^{-3})	LWP (g m^2)	TWP (g m^2)	AOD (–)	CF (–)
2008_1×	0.49	0.70	0.30	0.57	0.68	0.66	0.68	0.45	0.45	0.40	0.26	0.02	0.88	0.01
2008_PH2km	0.49	0.70	0.30	0.57	0.65	0.66	0.68	0.45	0.45	0.40	0.26	0.01	0.88	0.01
2018_1×	0.01	0.29	0.65	0.57	0.23	0.90	0.15	0.16	0.31	0.76	0.42	0.20	0.85	0.31

https://doi.org/10.5194/acp-2020-979
Preprint. Discussion started: 22 October 2020

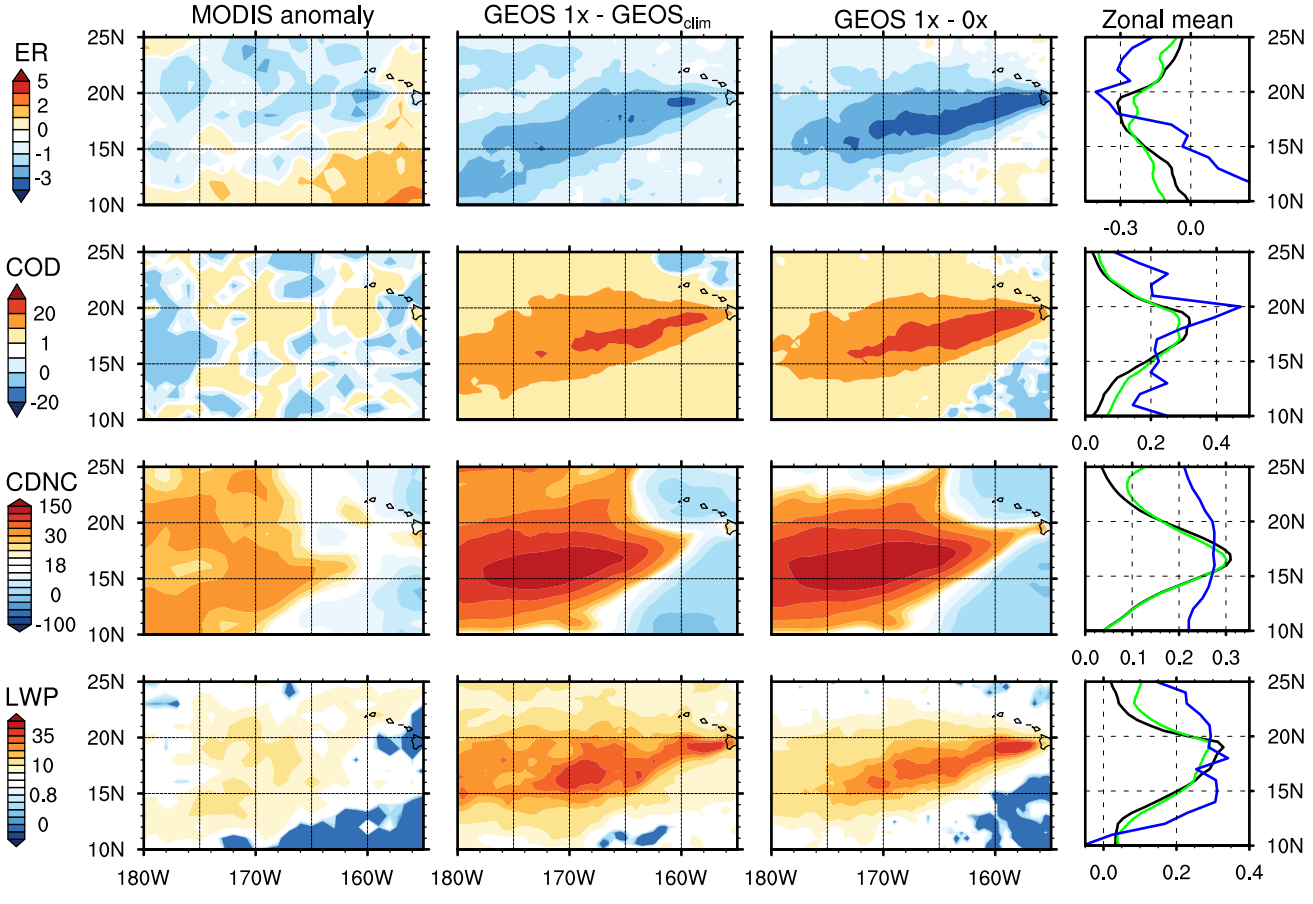

Figure 7. Like Fig. 6 but for MJJ 2018.

https://doi.org/10.5194/acp-2020-979
Preprint. Discussion started: 22 October 2020

Atmospheric Chemistry and Physics Discussions

5.0.2 Ice Clouds

It is likely that the degassing events introduced sulfate and ash particles to the upper troposphere; however, their effect on ice cloud development depends strongly on the microphysical processes dominating cloud evolution as well as the efficiency with which the new particles can promote ice crystal formation (Barahona et al., 2010). Figure 8 shows that during the 2008 event, the aerosol plume had little effect altering the properties of ice clouds. The 2008_1×−$\text{GEOS}_{\text{CLIM}}$ anomalies in ice clouds appeared spatially consistent with MODIS anomalies for COD and IWP, whereas the 2008_1×−0× showed little to no variability in the domain. This suggested that most of the observed anomaly results from meteorological and SST variability. Anomalous conditions in ice clouds with respect to climatological and background conditions, however, did not appear statistically significant (Table 4). GEOS anomaly estimates for the 2018_1× experiment appeared less spatially consistent with MODIS satellite retrievals for ice than for liquid clouds and had overall low correlations with MODIS observations (Table 5). Similar to the 2008 event, there seemed to be a strong meteorological component because the spatial correlation of the 2018_1×−$\text{GEOS}_{\text{CLIM}}$ results appeared more consistent with MODIS anomalies than for 2018_1×−2018_0×.

Domain anomalies for some variables stood out. As shown in Table 5, there was high correlation between MODIS and the 2008_1×−$\text{GEOS}_{\text{CLIM}}$ normalized zonal mean anomalies for COD ($R^2 = 0.84$) and IWP ($R^2 = 0.93$). These correlations substantially decreased when considering comparisons between MODIS and the 2008_1×−2008_0× difference. For COD in 2008, the latter seemed to retain some correlation ($R^2 = 0.29$), and may indicate some level of microphysical control on the observed anomalies. For 2018, there was a weak correlation between MODIS and the 2018_1×−$\text{GEOS}_{\text{CLIM}}$ anomaly for R_{eff}, COD and IWP. Whereas for R_{eff} and COD anomalous cloud properties appeared to be related to meteorological variability, the IWP correlation for MODIS vs. 2018_1×−2018_0× was slightly higher than against the climatology ($R^2 = 0.28$ vs. $R^2 = 0.20$); we found this difference to be significant at the 95% confidence level. The MODIS and $\text{GEOS}_{\text{CLIM}}$ anomalies for IWP in 2018 were of the same order of magnitude, $25.8\,\text{g}\,\text{m}^{-2}$ and $31.4\,\text{g}\,\text{m}^{-2}$, respectively (Table 4), whereas the GEOS IWP 2018_1×−2018_0× difference is $\approx 9.1\,\text{g}\,\text{m}^{-2}$. This strongly suggested a significant microphysical control on the IWP anomaly during the 2018 event.

https://doi.org/10.5194/acp-2020-979
Preprint. Discussion started: 22 October 2020

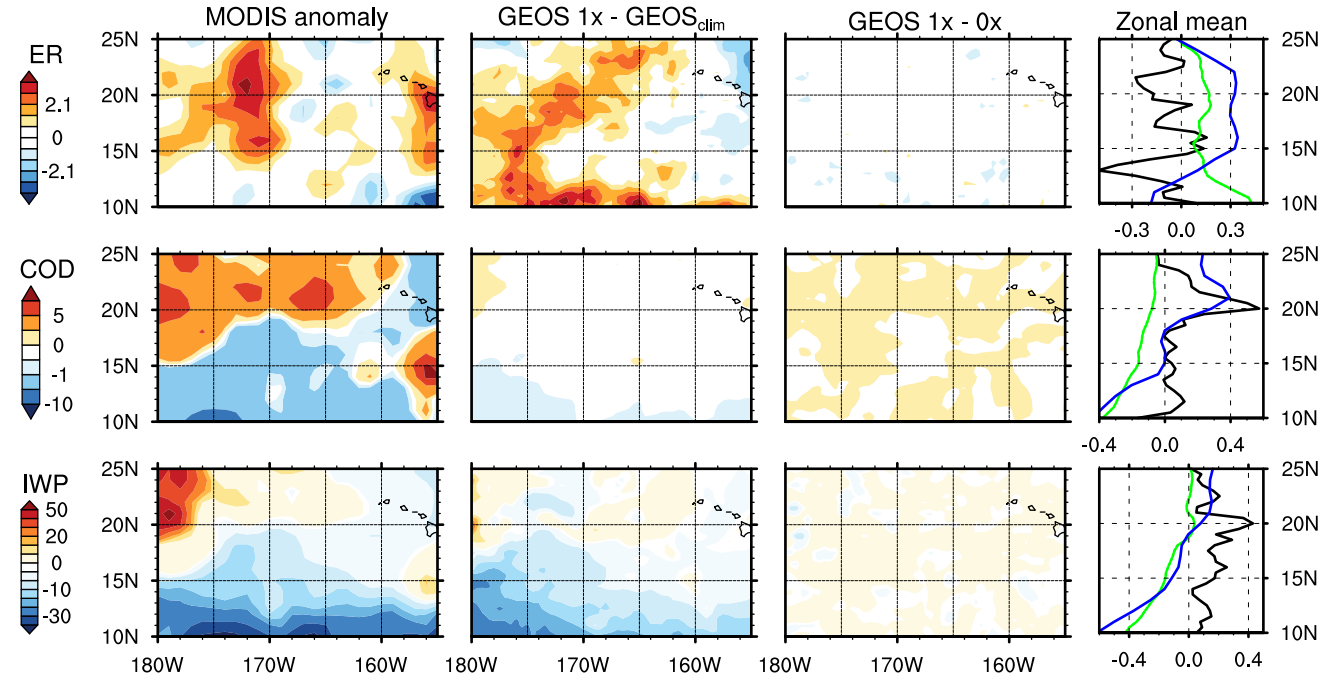

Figure 8. Ice cloud anomalies during JJA 2008 for (from top) R_{eff} (μm), COD (–), and IWP (g m^2). Anomalies are shown (from left) for MODIS observations, and for GEOS simulations calculated against GEOS$_{CLIM}$ and the zero emissions scenario. The rightmost column shows normalized zonal mean anomalies for MODIS (blue), and GEOS against GEOS$_{CLIM}$ (green) and zero emissions (black).

5.0.3 Role of injection height and ash content

Domain-averaged CDNC varied widely between the different experiments, except for the cases with elevated plume heights (2008_PH2km and 2018_PH4km), which essentially overlapped with the 2008_1× and 2018_1× experiments, respectively (Figures 10 and 11). Despite this, increasing the plume height produced sizable differences in some of the anomalies, particularly for ice clouds (Table 4) and for the 2018 event, although the effect was small. Similarities between MODIS and GEOS results for the 2008_5× and 2018_1× experiments on liquid clouds (Table 2) indicated that increased aerosol loadings during the 2008 event mimicked effects on liquid cloud formation during the 2018 event, most notably for CDNC and AOD. This showed that liquid cloud sensitivity to the first AIE was dominated by aerosol loadings as opposed to plume morphology during the 2008 event. Increasing plume height in concert with aerosol loadings exceeding 20 kt SO_2 day^{-1} (2018_PH4km) reduced the anomaly in IWP and COD by less than 5% relative to the 2018_1× experiment (Table 5). Similarly, accounting for ash INP (2018_PH4km_ash) slightly increased the COD and IWP anomalies (Table 4). Although it had opposite effects in ice crystal mixing ratio, Q_{ice}, and number concentration (ICNC), with the former lower, and the latter higher, than in the 2018_PH4km experiment (Figure 5). This is further analyzed in Section 5.1. The correlations between GEOS anomalies and MODIS for R_{eff} and COD in ice clouds improved slightly by the inclusion of ash INP (Table 5).

https://doi.org/10.5194/acp-2020-979
Preprint. Discussion started: 22 October 2020

Atmospheric Chemistry and Physics Discussions

Table 4. Anomalies for ice cloud properties. Values in parentheses are the *p*-values associated with a one-sided Student's *t*-test against the long-term mean.

Experiment	Exp vs. climatology			Exp vs. 0×		
	R_{eff} (μm)	COD (–)	IWP (g m^2)	R_{eff} (μm)	COD (–)	IWP (g m^2)
2008_1×	0.25 (0.73)	-0.13 (0.19)	-0.46 (0.80)	-0.04 (0.96)	0.00 (0.99)	0.35 (0.85)
MODIS (2008)	0.53 (0.60)	0.79 (0.40)	-1.46 (0.55)	– (–)	– (–)	– (–)
2018_1×	1.24 (0.29)	0.61 (0.20)	31.44 (0.16)	0.19 (0.85)	0.07 (0.85)	9.06 (0.59)
2018_PH4km	1.12 (0.32)	0.58 (0.20)	30.38 (0.16)	0.08 (0.94)	0.04 (0.90)	8.00 (0.62)
2018_PH4km_ash	-4.33 (0.01)	0.63 (0.18)	36.44 (0.15)	-5.38 (0.01)	0.10 (0.79)	14.06 (0.47)
MODIS (2018)	0.00 (0.27)	3.03 (0.18)	20.59 (0.26)	– (–)	– (–)	– (–)

Table 5. Linear coefficients of determination comparing GEOS normalized zonal anomalies for ice clouds against MODIS.

Experiment	MODIS anomaly vs GEOS 1×−clim			MODIS anomaly vs GEOS 1× vs. 0×		
	R_{eff} (μm)	COD (–)	IWP (g m^2)	R_{eff} (μm)	COD (–)	IWP (g m^2)
2008_1×	0.25	0.84	0.93	0.01	0.29	0.04
2018_1×	0.23	0.25	0.20	0.01	0.04	0.28
2018_PH4km	0.25	0.16	0.20	0.14	0.04	0.34
2018_PH4km_ash	0.27	0.39	0.15	0.29	0.01	0.21

https://doi.org/10.5194/acp-2020-979
Preprint. Discussion started: 22 October 2020

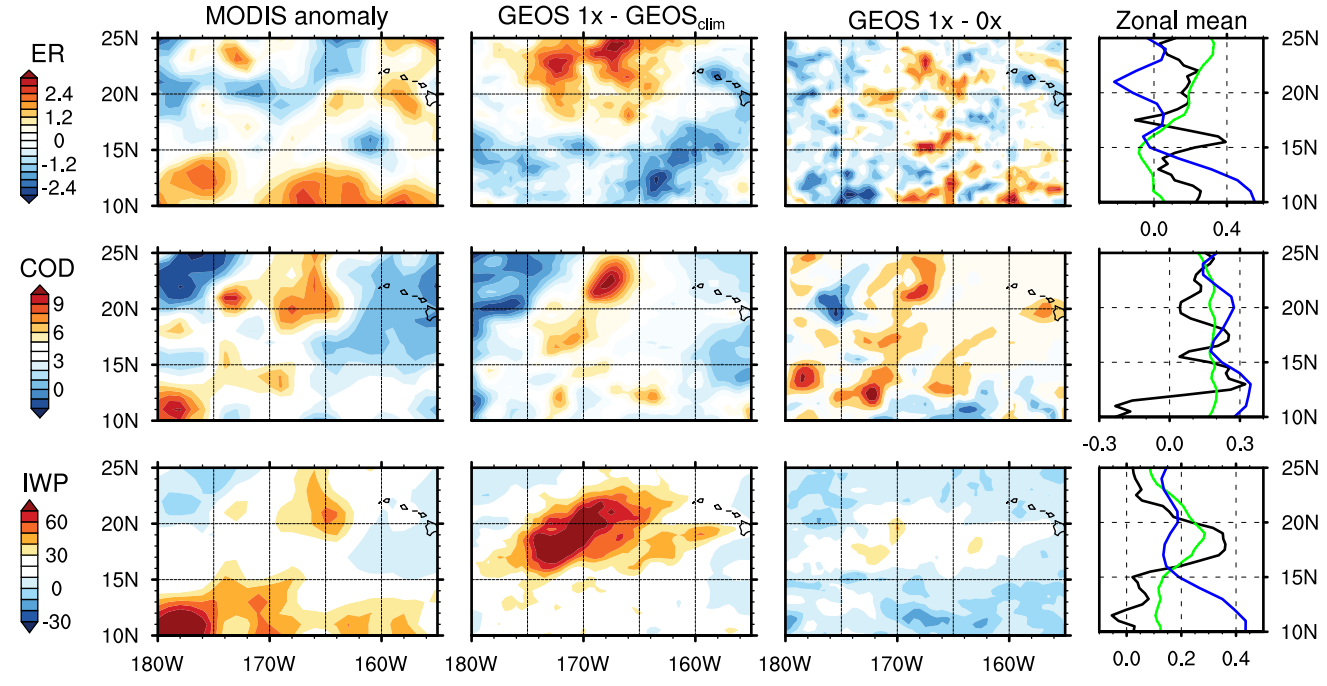

Figure 9. Like Fig.8 but for MJJ 2018

https://doi.org/10.5194/acp-2020-979
Preprint. Discussion started: 22 October 2020

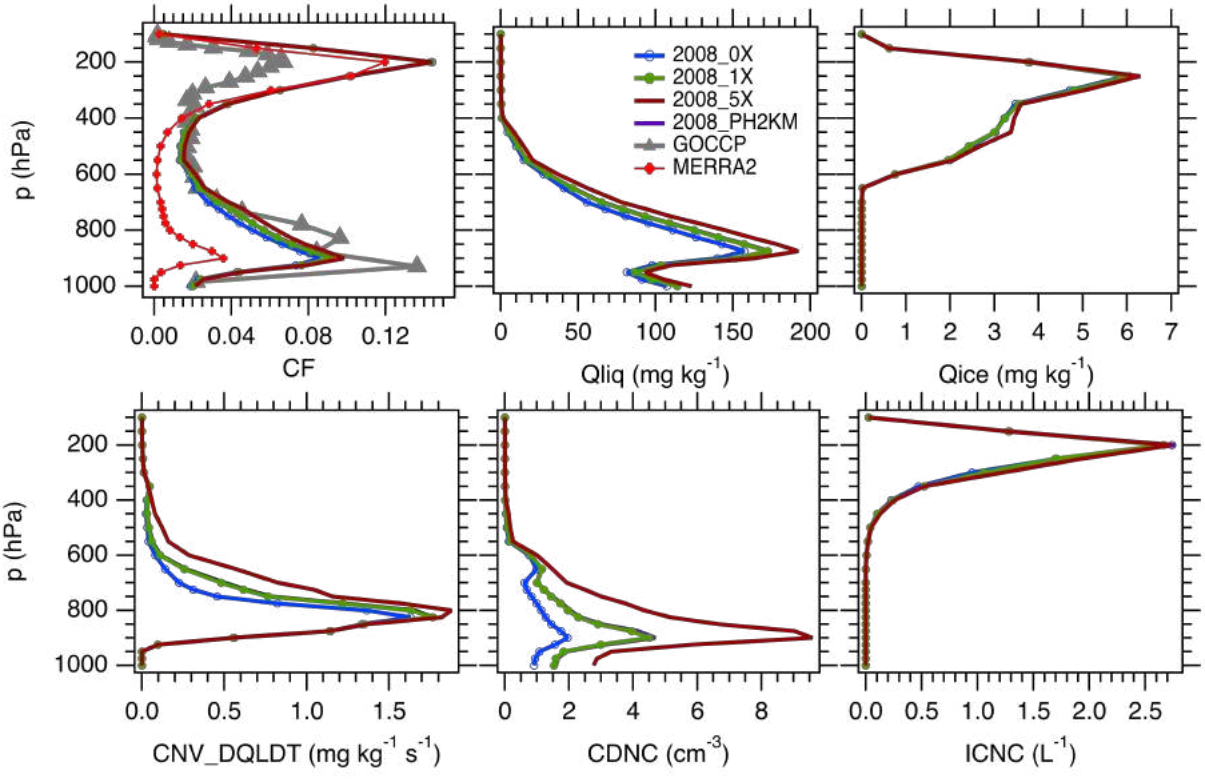

Figure 10. Zonal mean vertical profiles for cloud fraction (CF), liquid (Q_{liq}) and ice (Q_{ice}) mixing ratios, total detrained condensate tendency (CNV_DQLDT), cloud droplet (CDNC) and ice crystal (ICNC) number concentration, for the 2008 JJA season.

https://doi.org/10.5194/acp-2020-979
Preprint. Discussion started: 22 October 2020

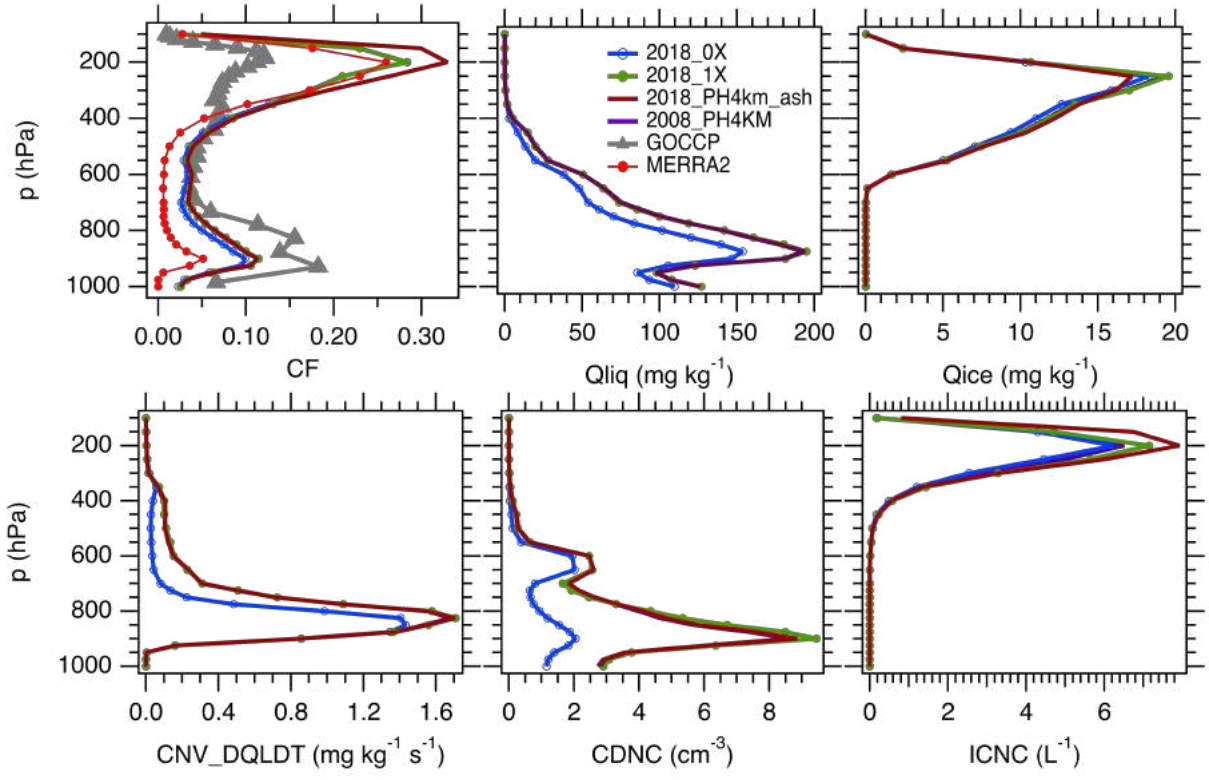

Figure 11. Equivalent to Figure 10 but for the 2018 MJJ season.

https://doi.org/10.5194/acp-2020-979
Preprint. Discussion started: 22 October 2020


Atmospheric Chemistry and Physics Discussions

5.1 Microphysical Controls on ACIs

Figures 10 and 11 summarize the experiments performed in this work. In all runs, and for both events, the vertical profile of cloud fraction was remarkably similar with two predominant cloud layers associated with shallow cumulus and warm cirrus/altocumulus. This vertical structure was in agreement with GOCCP data (also shown in Figures 4 and 5). Compared to GOCCP, GEOS however tended to overestimate high level CF and underestimated it near the surface. This was discussed in Section 5, however here we also note that there is a high uncertainty in the retrieval during these periods. For example, GEOS-simulated high-level clouds were in better agreement with MERRA-2, whereas low level cloud fraction in the latter was much lower than suggested by GOCCP. In both cases, CF around 800 hPa was slightly higher for high aerosol loading than for the no emissions experiments indicating deepening of the clouds from the injection of aerosol. This was supported by an increase in liquid water mixing ratio, Q_{liq}, between the 1× and the 0× experiments and runs along an enhanced detrained mass tendency, CNV_DQLDT, indicating predominant convective effects.

These effects can be understood in light of the modification to dominant microphysical tendencies by elevated aerosol emissions. Figures 12 and 13 show the seasonally averaged rates of different cloud microphysical processes that took place during each event. They are distinguished by processes that affect mass and number concentration of liquid droplets and ice crystals. Both events showed similar features regarding processes affecting liquid condensate and CDNC (panels (a) and (c) in Figs. 12 and 13). As expected, liquid cloud microphysics was dominated by CCN activation and condensation, i.e., by droplet formation on sulfate particles. Cumulus detrainment (DCNVL) is a significant source of condensate but only plays a minor role in determining CDNC. The main sinks of liquid mass and number concentration are droplet autoconversion (AUT) and accretion of cloud droplets by rain (ACRL_RAIN). The CCN source rate in 2018 (Fig. 13 c) was about 3× that of 2008 (Fig. 12); however, the liquid condensate tendencies, panel (a) in both figures, were of the same magnitude. Thus the mechanism for the decrease in R_{eff} was an increase in CCN activation, hence CDNC, which did not translate into a proportional increase in liquid mass, i. e., the first AIE. This is revealed in Figs. 10 and 11 as large increases in CDNC, but only slight increases in Q_{liq}, between the 1× and the 0× experiments.

It is not clear why the liquid AUT sinks were almost insensitive to the aerosol load. Most likely, the liquid mass and number concentration sinks were controlled by accretion rather than autoconversion. This is depicted in Fig. 14. Panels (a) and (c) show that the autoconversion sinks for mass and number were similar across all simulation experiments, even those without volcanic emissions (i.e., 2008_0× and 2018_0×), despite CCN activation tendencies varying by a factor of 4. Accretion by rain (ACRL_RAIN) was, however, enhanced for GEOS experiments with high aerosol concentrations (Fig. 14 c). This suggested an unexpected mechanism for the enhanced LWP. Ingestion of CCN within convective parcels inhibits the formation of precipitation in cumulus clouds; hence more condensate was detrained to the top. DCNVL was thus enhanced in simulations with high aerosol loading (2018_1×, 2008_1×, and 2008_5× in Fig. 14 a). This was reflected in the vertical profiles of total detrained tendency (CNV_DQLDT), Q_{liq}, and to a lesser extent in CF (Figs. 10 and 11). This mechanism created deeper clouds that precipitated from above scavenging the liquid below, which explained the increase in ACRL_RAIN as the CCN activation tendency increases. Because droplets also freeze higher in the convective parcel it may also lead to convective invigoration,

https://doi.org/10.5194/acp-2020-979
Preprint. Discussion started: 22 October 2020


Atmospheric Chemistry and Physics Discussions

although our setup (i.e., replaying T) prevented GEOS from explicitly simulating this. These findings are consistent with the deepening of the cloud layers described by Yuan et al. (2011) and the evidence for convective invigoration reported by Mace and Abernathy (2016). They also explain the anomalous enhancement of the mid-level CF and the increased SCF during the two events found in the GOCCP retrievals (Figs. 4 and 5).

Whereas a few processes dominate the microphysics of liquid water, ice microphysics is much more complex. It is clear from Figs. 10 and 11 that ice nucleation (ICENUC), sedimentation (SDM), and growth/sublimation (DEP) were dominant. However other processes, notably convective detrainment (DCNVI) and the Weneger-Bergeron-Findeisen (WBF) process, still played significant roles in cloud development. Ice autoconversion to snow (AUTICE) was a significant sink for ice mass but not for number concentration. It is likely that the latter was controlled by SDM. This complex microphysical make up may be one of the reasons why the anomalies for ice clouds were much less evident than for liquid clouds, buffering the former against aerosol perturbations.

It is also interesting that almost every ice tendency was 2–3× larger in the 2018 (Fig. 13) than in the 2008 event (Fig. 12), while the liquid condensate rates were of the same magnitude across all experiments (Fig. 14). The main reason for this was that Q_{ice} was larger in 2018 than in 2008 (Figs. 10 and 11), likely due to higher SSTs during neutral ENSO conditions relative to La Niña SST cooling in 2008. Warmer SSTs triggered more frequent convection events and enhanced the transport of condensate, water vapor, and frozen condensate to the upper troposphere. Crystals sedimenting from above find a favorable environment to grow (which also enhances splintering processes below, represented by HM in Fig. 13). Although there was definitely a higher ice crystal nucleation rate (ICENUC) in 2018 than in 2008 (Figure 14), the fact that it changed little upon modification of the injection height or by considering ash as INP, strongly suggested that changes in the vertical transport of liquid and water vapor, rather than ICENUC, led to the observed anomalies in ice clouds. In fact, accounting for ash INP had a negligible effect on immersion freezing rates (not shown). Including ash INP led to slightly higher ice nucleation rates between 200–300 hPa. Because these crystals grow and sediment quickly, these may explain the slightly lower Q_{ice} values with respect to the 2018_1× experiment despite the higher ICNC (Fig. 11).

https://doi.org/10.5194/acp-2020-979
Preprint. Discussion started: 22 October 2020

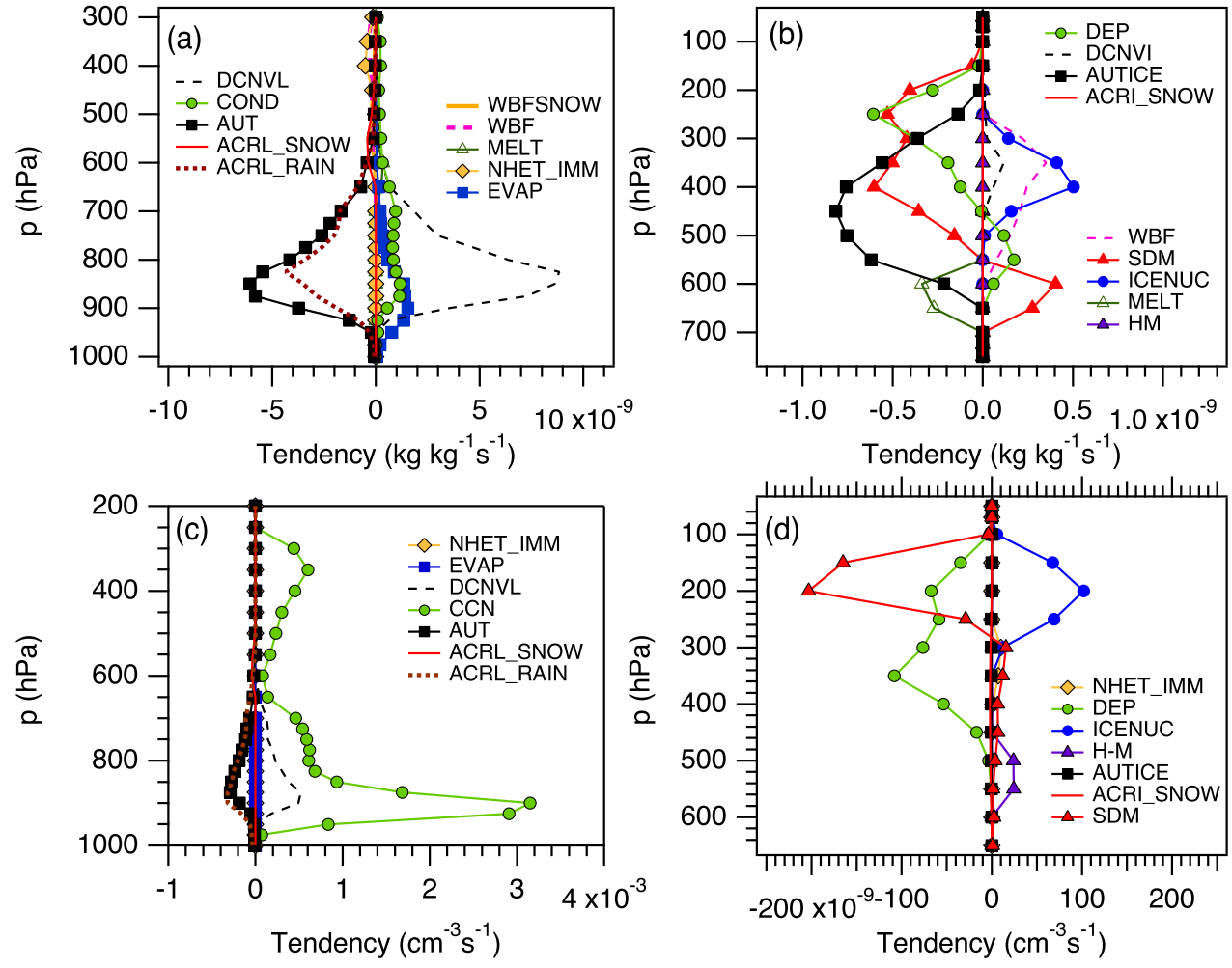

Figure 12. Domain-averaged cloud microphysical tendencies for the 2008 JJA season, for (a) liquid mass, (b) ice mass, (c) liquid number, and (d) ice number concentration. Shown are Bergeron-Findeisen process on ice (WBF) and snow (WBFSNOW), melting (MELT), total ice nucleation, and by immersion freezing only (ICENUC and NHET_IMM, respectively), droplet evaporation (EVAP), convective detrainment of liquid and ice (DCNVL and DCNVI), condensation (COND), liquid and ice autoconversion (AUT and AUTICE, respectively), accretion of liquid by rain and snow (ACRS and ACRL, respectively), CCN activation (CCN), ice sedimentation (SDM), ice crystal growth and accretion by snow (DEP, ACRI_SNOW, respectively), and ice splintering (HM).

https://doi.org/10.5194/acp-2020-979
Preprint. Discussion started: 22 October 2020

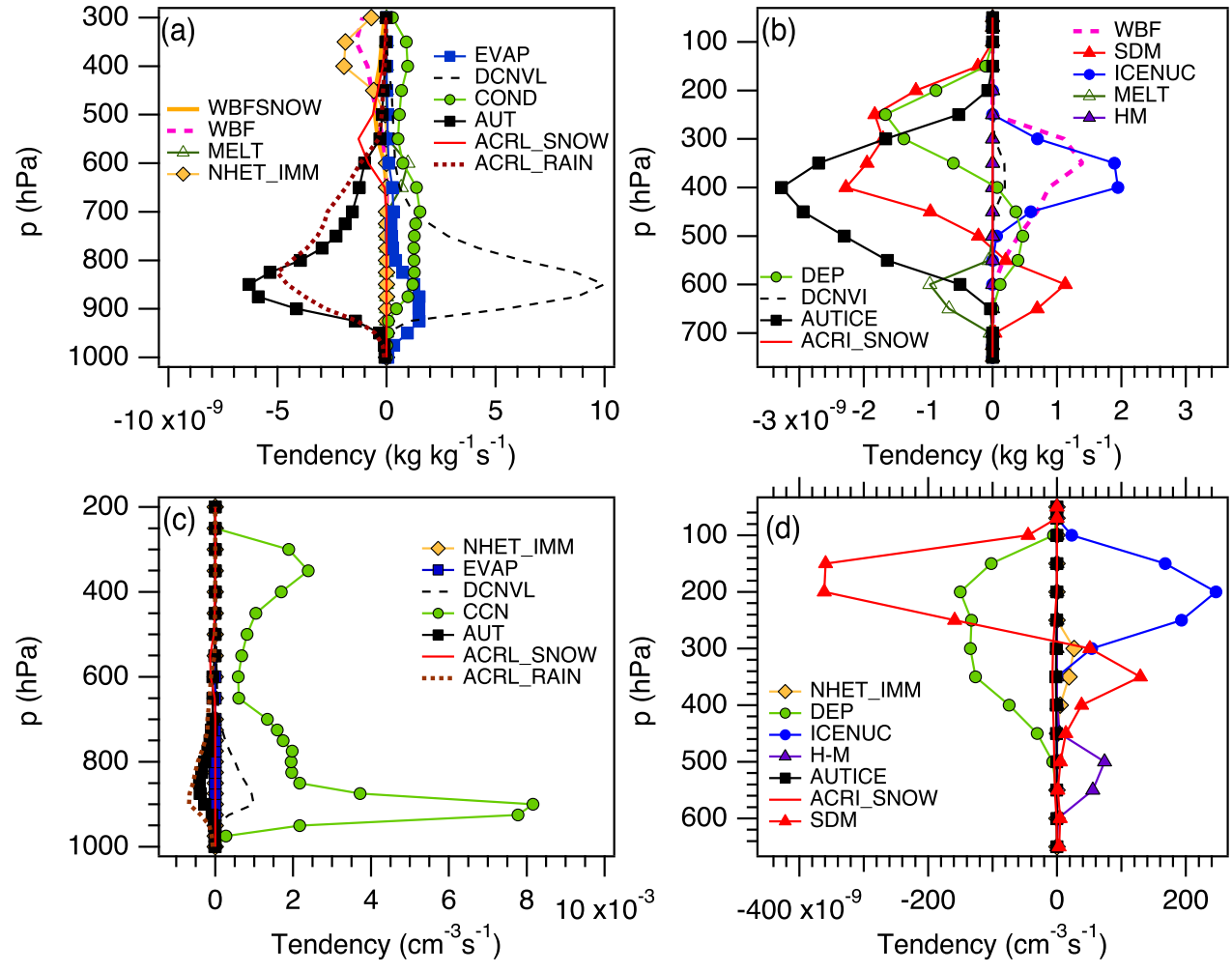

Figure 13. Like Fig. 12 but for the 2018 MJJ season.

https://doi.org/10.5194/acp-2020-979
Preprint. Discussion started: 22 October 2020

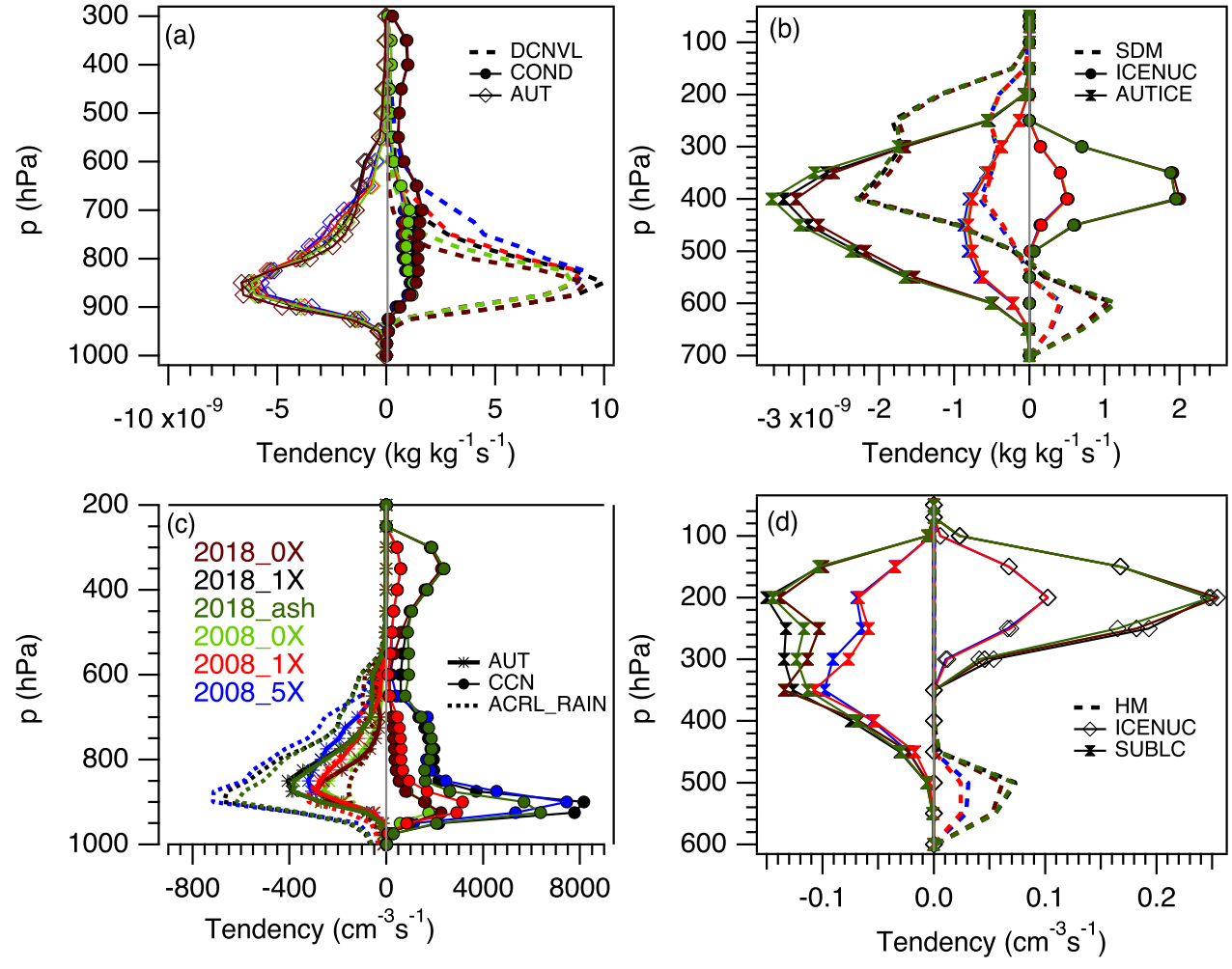

Figure 14. Comparison of dominant microphysical process rates for (a) liquid mass, (b) ice mass, (c) liquid number, and (d) ice number concentration for the experiments listed in Table 1.

https://doi.org/10.5194/acp-2020-979
Preprint. Discussion started: 22 October 2020


Atmospheric Chemistry and Physics Discussions

6 Conclusions

We carried out a comprehensive analysis of the effects of aerosol emissions on cloud formation and microphysical properties during two major volcanic events from the Kilauea summit crater, Halemaumau, in the Hawaiian islands, occurring during the late spring and summer of 2008 and 2018. This is the first time that such an analysis has been performed for the 2018 event. We combined satellite data, reanalysis products, and AGCM simulations to analyze and understand the role of meteorology and microphysics in determining the effects of volcanic aerosol emissions on cloud properties.

The 2018 Kilauea degassing event was stronger and more regionally significant with respect to cloud formation processes for both liquid and ice clouds, while the 2008 event affected liquid clouds only. For liquid clouds, the 2008_5× emissions scenario was similar to modeled and observed conditions for the 2018_1× simulation. This indicated that effects on liquid clouds simulated by GEOS were dominated by elevated SO_2 concentrations. For ice clouds, changes in cloud microphysics were significant following the 2018 event while few, if any, effects were apparent in the 2008 event. Several factors contributed to observed and simulated similarities/differences for each event: (1) aerosol loading, (2) plume height and composition, and (3) ENSO conditions. Observations confirmed that aerosol concentrations were anomalously high during both events relative to long-term means and zero-emissions simulations. The aerosol emissions source was the Kilauea Volcano and the plume extended westward across the domain driven by easterly trade winds. The 2018 emissions were $\geq 5\times$ higher than emissions in 2008, although differences between GEOS 2008_5× and 2018_1× experiments indicated that conditions other than aerosol loading caused macro- and microphysical effects on clouds during the 2018 event.

Both events suggested possible constraints for AIEs in satellite retrievals and model simulations. The ACI signatures common to both events suggested that effects on cloud macro- and microphysical properties with respect to the first indirect effect, such as increased CCN, were likely decoupled from local meteorological effects. In contrast, changes in precipitation efficiency and cloud lifetime in the presence of increased aerosol concentrations were likely dampened by meteorological variability. Thus even in well-constrained natural experiments as the ones presented in this paper, caution must be taken when drawing conclusions on the second indirect effect without full consideration of meteorological effects.

Both MODIS and GEOS showed large positive anomalies for IWP and COD during 2018 across the domain, which indicated that conditions favorable for ice cloud formation present in 2018 were absent in 2008. Ash was present in the volcanic plume for both degassing events, but only the plume in 2018 injected volcanic material to sufficiently high altitudes to potentially impact the formation of ice clouds. Sensitivity experiments using increased emissions, plume height, and introducing ash as INP suggested that these changes only slightly amplified anomalies for both liquid and ice clouds.

We performed a detailed analysis of the rates of cloud microphysical processes during the two events. As expected, CCN activation played a major role in determining the cloud droplet number concentration for both cases; however, increased CDNC did not lead to increased cloud water content. Instead, ingestion of CCN within convective parcels led to detrainment of condensate at higher levels, which may have caused convective invigoration. As a result, clouds perturbed by aerosols were optically deeper than in the pristine cases. This mechanism also led to enhanced cloud droplet scavenging by accretion.

https://doi.org/10.5194/acp-2020-979
Preprint. Discussion started: 22 October 2020


Atmospheric Chemistry and Physics Discussions

Microphysical rates in ice clouds were found to be accelerated in 2018 with respect to 2008, likely resulting from a higher SST during El Niño conditions in the former (hence more convective inflow to the upper troposphere) and by an increase in convective detrainment in the presence of aerosols. Although the ice nucleation rate in cirrus clouds was substantially higher in 2018 than in 2008, it is likely that it did not control the observed anomaly in ice cloud properties in the former. Accounting for ice formation on ash INP lead to slightly enhanced ice nucleation in warm cirrus clouds thereby facilitating ice sedimentation and decreasing ice water content.

This work showed that satellite observations provided strong evidence for the effects of aerosols modifying clouds during the Kilauea volcanic events. GEOS simulations elucidated the mechanisms of and provided insight into the microphysical processes involved in aerosol cloud interactions. Additionally, we showed that there were many similarities between the 2008 and 2018 degassing events. Although the model configuration used in this work presented a clear view of the role of different microphysical processes in determining the evolution of clouds during the 2008 and 2018 events, it precluded a full exploration of the second indirect effect and the simulation of convective invigoration. These effects will be explored in future studies. Future work would also look at the feedbacks between aerosol loading and SST. Our work however provided an unprecedented view of the mechanisms driving the aerosol indirect effect during volcanic events, helping to advance the understanding of the role of aerosol emissions on climate.

Author contributions. D. Barahona conceived and supervised this work. K.H. Breen prepared the GEOS simulations and the analysis of the satellite retrievals. H. Bian. and T. Yuan contributed daily emissions files for the volcanic events. S. C. James contributed as a scientific consultant and editor of the manuscript.

Competing interests. No competing interests are present.

Acknowledgements. D. Barahona was partially supported by the NASA Modeling and Analysis Program, Grant 15-CCST15-0066. Part of this work was performed during K.H. Breen's summer 2019 internship at NASA GSFC. We thank Mian Chin and Kai Yang for providing SO_2 emissions data. All authors have read and agreed to the published version of the manuscript. All maps were generated using the NCAR Command Language (Version 6.3.0) Software. (2016). Boulder, Colorado: UCAR/NCAR/CISL/TDD. http://dx.doi.org/10.5065/D6WD3XH5.

https://doi.org/10.5194/acp-2020-979
Preprint. Discussion started: 22 October 2020

Atmospheric Chemistry and Physics Discussions

Appendix A: Ice nucleation on ash particles

SO_2 is the primary aerosol associated with volcanic degassing events. There is, however, evidence that ash was co-emitted with sulfate at the Kilauea Volcano, which may have an effect on the way the plume interacts with clouds by introducing additional surfaces for ice nucleation (ash is typically considered a poor CCN) (Durant et al., 2008). Ash concentration was likely important during the 2018 event when particulate emissions reached the upper troposphere (Neal et al., 2019). To assess the impact of ash on ice cloud formation, the ice nucleation parameterization in GEOS was amended as follows.

For mixed-phase clouds, ash was assumed to induce immersion freezing. Maters et al. (2019) reported the active site density, n_s, of tephra consisting of glassy lithic fragments and ash particles emitted from Kilauea in May 2018. Only ash particles were found to be active ice nucleation sites. For the ash samples, n_s (cm^{-2}) was fit as:

$$n_s = \exp\left(-0.6907T + 176.5992\right), \tag{A1}$$

with $240 \leq T \leq 260\,\mathrm{K}$, where T is temperature. Specific surface area was prescribed as $2.1\,\mathrm{m^2\,g^{-1}}$ (Maters et al., 2019). Ash content in the volcanic plume was assumed to be 0.1%, consistent with literature values (Mastin et al., 2009).

Ash was also assumed to heterogeneously nucleate ice in the deposition mode at low temperature ($T < 236\,\mathrm{K}$) hence affecting the formation of cirrus clouds. Although the ice nucleation efficiency of ash from the Kilauea summit crater has not been reported, Hoyle et al. (2011) measured a saturation freezing threshold of 110% for ash emissions from the Eyjafjallajökull volcano. This value is used as a first approximation for the Kilauea ash emissions. Ash was then treated as a monodisperse INP (Barahona and Nenes, 2009b) and added to the Ullrich et al. (2017) ice nucleation spectrum. The nucleated ice crystal concentration was then calculated using the Barahona and Nenes (2009a) parameterization.

https://doi.org/10.5194/acp-2020-979
Preprint. Discussion started: 22 October 2020

Atmospheric Chemistry and Physics Discussions

References

Abdul-Razzak, H. and Ghan, S.: A parameterization of aerosol activation, 2. Multiple aerosol types., J. Geophys. Res., 105, 6837–6844, doi:10.1029/1999JD901 161, 2000.

Albrecht, B. A.: Aerosols, cloud microphysics, and fractional cloudiness, Science, 245, 1227–1230, 1989.

Barahona, D. and Nenes, A.: Parameterizing the competition between homogeneous and heterogeneous freezing in cirrus cloud formation - polydisperse ice nuclei, Atmospheric Chemistry & Physics, 9, 5933–5948, 2009a.

Barahona, D. and Nenes, A.: Parameterizing the competition between homogeneous and heterogeneous freezing in cirrus cloud formation - monodisperse ice nuclei, Atmos. Chem. Phys., 9, 369–381, 2009b.

Barahona, D., Rodriguez, J., and Nenes, A.: Sensitivity of the global distribution of cirrus ice crystal concentration to heterogeneous freezing, J. Geophys. Res.: Atmospheres, 115, 2010.

Barahona, D., Molod, A., Bacmeister, J., Nenes, A., Gettelman, A., Morrison, H., Phillips, V., and Eichmann, A.: Development of two-moment cloud microphysics for liquid and ice within the NASA Goddard Earth Observing System Model (GEOS-5), Geosc. Model Dev., 7, 1733–1766, https://doi.org/10.5194/gmd-7-1733-2014, http://www.geosci-model-dev.net/7/1733/2014/, 2014.

Barahona, D., Molod, A., and Kalesse, H.: Direct estimation of the global distribution of vertical velocity within cirrus clouds, Scientific Reports, 7, 6840, https://doi.org/10.1038/s41598-017-07038-6, 2017.

Beirle, S., Hörmann, C., Penning de Vries, M., Dörner, S., Kern, C., and Wagner, T.: Estimating the volcanic emission rate and atmospheric lifetime of SO_2 from space: a case study for Kīlauea volcano, Hawaii, Atmospheric Chemistry and Physics, 14, 8309–8322, 2014.

Bender, F.-M., Frey, L., McCoy, D. T., Grosvenor, D. P., and Mohrmann, J. K.: Assessment of aerosol–cloud–radiation correlations in satellite observations, climate models and reanalysis, Climate Dynamics, 52, 4371–4392, 2019.

Bennartz, R.: Global assessment of marine boundary layer cloud droplet number concentration from satellite, Journal of Geophysical Research: Atmospheres, 112, 2007.

Bennartz, R. and Rausch, J.: Global and regional estimates of warm cloud droplet number concentration based on 13 years of AQUA-MODIS observations, Atmospheric Chemistry and Physics, 17, 9815, 2017.

Boo, K.-O., Booth, B. B., Byun, Y.-H., Lee, J., Cho, C., Shim, S., and Kim, K.-T.: Influence of aerosols in multidecadal SST variability simulations over the North Pacific, Journal of Geophysical Research: Atmospheres, 120, 517–531, 2015.

Boucher, O., Randall, D., Artaxo, P., Bretherton, C., Feingold, G., Forster, P., Kerminen, V.-M., Kondo, Y., Liao, H., Lohmann, U., Rasch, P., Satheesh, S., Sherwood, S., Stevens, B., and Zhang, X.: in: Climate Change 2013: The Physical Science Basis. Contribution of Working Group I to the Fifth Assessment Report of the Intergovernmental Panel on Climate Change: Clouds and Aerosols, edited by Stocker, T., Qin, D., Plattner, G.-K., Tignor, M., Allen, S., Boschung, J., Nauels, A., Xia, Y., Bex, V., and Midgley, P., pp. 571–657, Cambridge University Press, Cambridge, United Kingdom and New York, NY, USA, 2013.

Carn, S., Yang, K., Prata, A., and Krotkov, N.: Extending the long-term record of volcanic SO_2 emissions with the Ozone Mapping and Profiler Suite nadir mapper, Geophysical Research Letters, 42, 925–932, 2015.

Carn, S., Fioletov, V., McLinden, C., Li, C., and Krotkov, N.: A decade of global volcanic SO_2 emissions measured from space, Scientific reports, 7, 44 095, 2017.

Chepfer, H., Bony, S., Winker, D., Cesana, G., Dufresne, J., Minnis, P., Stubenrauch, C., and Zeng, S.: The GCM-oriented CALIPSO cloud product (CALIPSO-GOCCP), Journal of Geophysical Research: Atmospheres, 115, 2010.

https://doi.org/10.5194/acp-2020-979
Preprint. Discussion started: 22 October 2020

Colarco, P., da Silva, A., Chin, M., and Diehl, T.: Online simulations of global aerosol distributions in the NASA GEOS-4 model and comparisons to satellite and ground-based aerosol optical depth, J. Geophys. Res., 115, D14 207–, http://dx.doi.org/10.1029/2009JD012820, 2010.

Durant, A. J., Shaw, R., Rose, W. I., Mi, Y., and Ernst, G.: Ice nucleation and overseeding of ice in volcanic clouds, Journal of Geophysical Research: Atmospheres, 113, 2008.

Eguchi, K., Uno, I., Yumimoto, K., Takemura, T., Nakajima, T. Y., Uematsu, M., and Liu, Z.: Modulation of cloud droplets and radiation over the North Pacific by sulfate aerosol erupted from Mount Kilauea, SOLA, 7, 77–80, 2011.

Elias, T. and Sutton, A. J.: Sulfur dioxide emission rates from Kīlauea Volcano, Hawai 'i, 2007–2010, Tech. rep., US Geological Survey, 2012.

Elias, T., Kern, C., Horton, K., Sutton, A. J., and Garbeil, H.: Measuring SO_2 emission rates at Kīlauea Volcano, Hawaii USA, 2014-2017, Frontiers in Earth Science, 6, 214, 2018.

Gelaro, R., McCarty, W., Suárez, M. J., Todling, R., Molod, A., Takacs, L., Randles, C. A., Darmenov, A., Bosilovich, M. G., Reichle, R., et al.: The modern-era retrospective analysis for research and applications, version 2 (MERRA-2), J. Climate, 30, 5419–5454, 2017.

Gryspeerdt, E., Quaas, J., Ferrachat, S., Gettelman, A., Ghan, S., Lohmann, U., Morrison, H., Neubauer, D., Partridge, D. G., Stier, P., et al.: Constraining the instantaneous aerosol influence on cloud albedo, Proc. Nat. Acad. Sci. USA., 114, 4899–4904, 2017.

Hoyle, C. R., Pinti, V., Welti, A., Zobrist, B., Marcolli, C., Luo, B., Höskuldsson, Á., Mattsson, H. B., Stetzer, O., Thorsteinsson, T., et al.: Ice nucleation properties of volcanic ash from Eyjafjallajökull, Atmospheric Chemistry and Physics, 11, 9911–9926, 2011.

Koren, I., Kaufman, Y. J., Rosenfeld, D., Remer, L. A., and Rudich, Y.: Aerosol invigoration and restructuring of Atlantic convective clouds, Geophys. Res. Lett., 32, 2005.

Lohmann, U. and Feichter, J.: Global indirect aerosol effects: a review, Atmospheric Chemistry and Physics, 5, 715–737, 2005.

Mace, G. and Abernathy, A.: Observational evidence for aerosol invigoration in shallow cumulus downstream of Mount Kilauea, Geophysical Research Letters, 43, 2981–2988, 2016.

Malavelle, F. F., Haywood, J. M., Jones, A., Gettelman, A., Clarisse, L., Bauduin, S., Allan, R. P., Karset, I. H. H., Kristjánsson, J. E., Oreopoulos, L., et al.: Strong constraints on aerosol–cloud interactions from volcanic eruptions, Nature, 546, 485, 2017.

Mastin, L. G., Guffanti, M., Servranckx, R., Webley, P., Barsotti, S., Dean, K., Durant, A., Ewert, J. W., Neri, A., Rose, W. I., et al.: A multidisciplinary effort to assign realistic source parameters to models of volcanic ash-cloud transport and dispersion during eruptions, Journal of Volcanology and Geothermal Research, 186, 10–21, 2009.

Maters, E. C., Dingwell, D. B., Cimarelli, C., Müller, D., Whale, T. F., and Murray, B. J.: The importance of crystalline phases in ice nucleation by volcanic ash, Atmospheric Chemistry and Physics, 19, 5451–5465, 2019.

Molod, A., Takacs, L., Suarez, M., and Bacmeister, J.: Development of the GEOS-5 atmospheric general circulation model: evolution from MERRA to MERRA2, Geosc. Model Dev., 8, 1339–1356, https://doi.org/10.5194/gmd-8-1339-2015, 2015.

Morrison, H. and Gettelman, A.: A New Two-Moment Bulk Stratiform Cloud Microphysics Scheme in the Community Atmosphere Model, Version 3 (CAM3). Part I: Description and Numerical Tests, J. Clim., 21, 3642–3659, https://doi.org/10.1175/2008JCLI2105.1, http://journals.ametsoc.org/doi/abs/10.1175/2008JCLI2105.1, 2008.

Nadeau, P. A., Werner, C. A., Waite, G. P., Carn, S. A., Brewer, I. D., Elias, T., Sutton, A. J., and Kern, C.: Using SO_2 camera imagery and seismicity to examine degassing and gas accumulation at Kīlauea Volcano, May 2010, Journal of Volcanology and Geothermal Research, 300, 70–80, 2015.

https://doi.org/10.5194/acp-2020-979
Preprint. Discussion started: 22 October 2020

Neal, C., Brantley, S., Antolik, L., Babb, J., Burgess, M., Calles, K., Cappos, M., Chang, J., Conway, S., Desmither, L., et al.: The 2018 rift eruption and summit collapse of Kīlauea Volcano, Science, 363, 367–374, 2019.

Patrick, M., Dietterich, H., Lyons, J., Diefenbach, A., Parcheta, C., Anderson, K., Namiki, A., Sumita, I., Shiro, B., and Kauahikaua, J.: Cyclic lava effusion during the 2018 eruption of Kīlauea Volcano, Science, 366, 2019.

Potter, L., Kreidenweis, S., Huebert, B., Howell, S., Zhuang, J., and Morman, M.: Variability of sulfate aerosol concentrations at Mauna Loa observatory, Hawaii, in: AIP Conference Proceedings, vol. 1527, pp. 519–522, American Institute of Physics, 2013.

Randles, C. A., da Silva, A. M., Buchard, V., Colarco, P. R., Darmenov, A., Govindaraju, R., Smirnov, A., Holben, B., Ferrare, R., Hair, J., Shinozuka, Y., and Flynn, C. J.: The MERRA-2 Aerosol Reanalysis, 1980 Onward. Part I: System Description and Data Assimilation Evaluation, Journal of Climate, 30, 6823–6850, https://doi.org/10.1175/JCLI-D-16-0609.1, https://doi.org/10.1175/JCLI-D-16-0609.1, 2017.

Reynolds, R. W., Rayner, N. A., Smith, T. M., Stokes, D. C., and Wang, W.: An improved in situ and satellite SST analysis for climate, J. Climate, 15, 1609–1625, 2002.

Rienecker, M., Suarez, M., Todling, R., Bacmeister, J., Takacs, L., Liu, H.-C., Gu, W., Sienkiewicz, M., Koster, R., Gelaro, R., Stajner, I., and Nielsen, J.: The GEOS-5 Data Assimilation System - Documentation of Versions 5.0.1, 5.1.0, and 5.2.0., vol. 27 of *Technical Report Series on Global Modeling and Data Assimilation*, NASA Goddard Space Flight Center, Greenbelt, MD, USA, 2008.

Seinfeld, J. H., Bretherton, C., Carslaw, K. S., Coe, H., DeMott, P. J., Dunlea, E. J., Feingold, G., Ghan, S., Guenther, A. B., Kahn, R., et al.: Improving our fundamental understanding of the role of aerosol- cloud interactions in the climate system, Proceedings of the National Academy of Sciences, 113, 5781–5790, 2016.

Takacs, L. L., Suárez, M. J., and Todling, R.: The stability of incremental analysis update, Monthly weather review, 146, 3259–3275, 2018.

Takahashi, C. and Watanabe, M.: Pacific trade winds accelerated by aerosol forcing over the past two decades, Nature Climate Change, 6, 768–772, 2016.

Team, C. P. C. I.: Historical El Niño/La Niña episodes (1950–present); Cold & Warm Episodes by Season, https://origin.cpc.ncep.noaa.gov/products/analysis_monitoring/ensostuff/ONI_v5.php, Updated June 4, 2020 (accessed June 10, 2020).

Twomey, S.: The influence of pollution on the shortwave albedo of clouds, Journal of the atmospheric sciences, 34, 1149–1152, 1977.

Ullrich, R., Hoose, C., Möhler, O., Niemand, M., Wagner, R., Höhler, K., Hiranuma, N., Saathoff, H., and Leisner, T.: A new ice nucleation active site parameterization for desert dust and soot, Journal of the Atmospheric Sciences, 74, 699–717, 2017.

Yuan, T., Remer, L., and Yu, H.: Microphysical, macrophysical and radiative signatures of volcanic aerosols in trade wind cumulus observed by the A-Train, Atmospheric Chemistry and Physics, 11, 7119–7132, https://doi.org/doi:10.5194/acp-11-7119-2011, 2011.